Journal of Current Science and Technology, May-August 2023 Vol. 13 No. 2, pp. 364-391

ISSN 2630-0656 (Online)

Cite this article: Kohnhorst, S. A. (2022, May). Supramolecular structure of five-coordinate [(4-methyl-2,6-dinitrophenolato)(octaethylporphinato)iron(III)] heme complex. *Journal of Current Science and Technology, 13*(2), 364-391. https://doi.org/10.59796/jcst.V13N2.2023.1752

Journal of Current Science and Technology

Journal homepage: https://jcst.rsu.ac.th

Supramolecular structure of five-coordinate [(4-methyl-2,6-dinitrophenolato)(octaethylporphinato)iron(III)] heme complex

Saifon A. Kohnhorst

Chemistry Program, Faculty of Science and Technology, Nakhon Ratchasima Rajabhat University, Nakhon Ratchasima 30000, Thailand

*Corresponding author; E-mail: saifon.k@nrru.ac.th

Received 10 September 2022; Revised 28 February 2023; Accepted 2 March 2023;
Published online 15 July 2023

Abstract

The crystallographic and spectroscopic characterization of the phenolate complex of [(4-methyl-2,6-dinitrophenolato)(2,3,7,8,12,13,17,18-octaethylporphinato)Fe(III)], [Fe^{III}(OEP)(DNOC)] is reported. The 4-methyl-2,6-dinitrophenol (DNOC) ligand was coordinating with the Fe^{III}(OEP) moiety through the phenylato-O-atom. The complex crystallizes in the triclinic *P*-1 with Z=2. The crystallographic information showed the average Fe—Np distance of 2.053(18) Å, with the Fe displacement from the 24 atoms porphyrin plane of 0.41(6) Å, and the Fe—O distance of 1.881(15) Å showing a five-coordinate square-pyramidal geometry. The characteristic of the formation of the Fe—O bond was found near 537 cm^{-1} for IR spectra and the ν_4 band was near 534 cm^{-1} for Raman spectra. The major supramolecular interactions involved an intermolecular hydrogen bond C—H···O with a minimum distance of 2.732(5) Å, and the shortest plane-plane contact distance of 3.689(3) Å. The FT-IR characteristic showed the new band near 3400 cm^{-1}, which was broadened due to the formation of hydrogen bonds. The role of these weak C—H···O hydrogen bonds concerted to stabilized the crystal packing in the heme complex. Thus, the number of excellent hydrogen bond acceptors of the axial ligand contributes to its supramolecular structure.

Keywords**:** *dinitrophenol; heme; hydrogen bond; Iron porphyrin; malaria; phenolate; supramolecular.*

1. Introduction

Metalloporphyrins are extensive and play an important biological role, e.g. in light harvesting, oxygen transport (Facchin et al., 2021), catalysts (Martin, Johnson, Mercado, Raugei, & Mayer, 2020; Panyanon et al., 2021), colorimetric and photometric biosensors (Norvaiša, Kielmann, & Senge, 2020), medicinal chemistry (Kingsbury, & Senge, 2020), synthetic biological receptor and supramolecular assemblies studied (Park, Hong, Lee, & Jang, 2021). These types of supramolecular interactions in biomolecules have a hierarchical three-dimensional (3D) structure and are dominated by intermolecular interactions, hydrogen bonding (Lee, Lee, Kim, Lee, & Jang, 2020), C—H···N, C—H···O, C—H···π (Rani et al., 2018), O—H···O and N—H···X (Dhifaoui et al., 2018a; 2018b; Norvaiša, Flanagan, Gibbons, & Senge, 2019). Understand that the noncovalent interactions (Park et al., 2021; Martin et al., 2020) such as electrostatic interactions, π–π stacking, steric interactions, and hydrogen bonding (Hu, Noll, Schulz, & Scheidt, 2018) are important in many biological and chemical reactions, especially the electrostatic ligand binding for both carbon dioxide reduction reaction and oxygen reduction reaction (Martin et al., 2020; Facchin, et al., 2021) in hemeprotein.

The octaethylporphyrin (OEP) heme has significantly more supramolecular interactions, particularly of the C—H···π type (Puntharod et al., 2010), than the tetraphenylporphyrin (TPP) hemes and spectra of the OEP hemes are significantly more similar to β-hematin than those of TPP hemes.

A distinguishing feature of β-hematin that led to more supramolecular interactions compared to the model systems was the O atoms in the propionic acid residues on β-hematin. A strategy to improve the OEP heme model system was to use axial ligands containing O atoms, the first choice being (picrato) OEP (Fe(III)), and indeed a better malaria pigment model complexes with a much better match spectroscopically, to malaria pigment, was produced (Puntharod et al., 2017). The five-coordinate picrato complex, first studied as the room temperature structure (Puntharod, 2008) and later as the 100K structure (Bhowmik, Dey, Sahoo, & Rath 2013), indeed engages in considerable C—H···π bonding. In addition to the normal abundance of C—H···π interactions, it exhibits a large number of C—H···O interactions similar to β-hematin. Thus, stimulating the interest in other axial ligands with abundant opportunities for porphyrin to ligand C—H···O interactions.

In addition to being model compounds for β-hematin, porphinato iron(III) complexes are of further interest due to their occurrence in biochemical systems. Sumner (1926) first crystallized an enzyme (urease), and shortly thereafter the enzyme catalase, the enzyme isolated and crystallized with contains iron (Sumner, & Dounce, 1937). Phenolatoporphyrinato iron(III) complexes entered the biochemical structural literature as the cytochrome c peroxidase with its tyrosine coordinated to the porphinato iron(III) active site (Edwards, Xuong, Hamlin, & Kraut, 1987). Additional examples of high-valent iron oxy-ligand heme complexes found in heme peroxidases, and catalases have been reviewed (Hersleth, Ryde, Rydberg, Görbitz, & Andersson, 2006; Kirkman, & Gaetani, 2007) and studied as model systems, as in the intermediate-spin phenolate(porphinato)iron(III) complexes studied as models of tyrosine to (porphinato)iron(III) center (Bhowmik et al., 2013; Sahoo, Quesne, de Visser, & Rath, 2015), as well as of mutant hemoprotein systems (Watanabe, Nakajima, & Ueno, 2007). A nice report on Z′=2 porphinato Fe(II) complex found that the complex on one crystallographically independent site is similar to a peroxidase (Hu et al., 2018). The Bhowmik et al., (2013) report also included the structural report of the 100K (picrato)(OEP)Fe(III) complex as noted above. Understanding this phenomenon will extend the recent packing analysis applied to the Fe^{III}(OEP)Cl systems (Kohnhorst, & Haller, 2014).

In this paper, new efforts to create crystalline iron(III) complex with axial ligand hydrogen bonding acceptors is discussed. The complex of [Fe^{III}(OEP)(DNOC)] was synthesized as part of malaria pigment model systems studied (Kohnhorst, & Haller, 2014; Puntharod et al., 2010; Puntharod et al., 2017). Analysis of structure and solid-state resonant-Raman spectra of a group of 5-coordinate high spin iron(III) OEP and TPP of heme (malaria pigment) model system led to the conclusion that supramolecular interactions play an integral role in the resonant Raman excitonic enhancement observed when applying near IR-infrared excitation wavelengths in β-hematin (Puntharod et al., 2010).

2. Objectives

The goal of this study is to examine the functional properties, proximate composition, energy content, color characteristics, and sensory attributes of *akara* and *senke* prepared from cowpea flour paste.

3. Materials and methods

All chemicals were purchased and used without purification. The synthesis reactions were performed a room temperature.

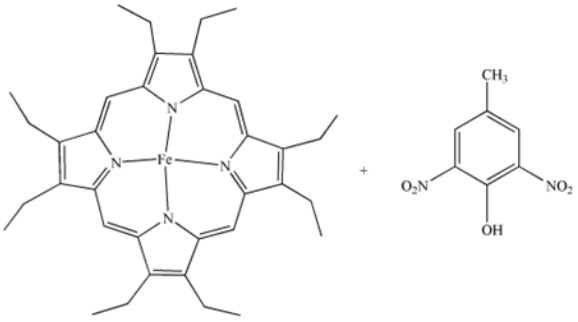

Figure 1 Schematic diagram of Fe^{III}(OEP)Cl and 4-methyl-2,6-dinitrophenol (DNOC) to form the title complex

The chlorido(2,3,7,8,12,13,17,18 octaethyl-porphyrinato)iron(III), Fe^{III}(OEP)Cl, and 4-methyl-2,6-dinitrophenol (DNOC) compound, the analytical grade of dimethylformamide (DMF), dimethylsulfoxide (DMSO) and chloroform ($CHCl_3$) were purchased from Sigma-Aldrich (USA) and used as received.

3.2 Synthesis of [Fe^{III}(OEP)(DNOC)]

The mixture of the title compound was prepared in the 1:2 molar ratio by dissolving 1.58 mg (2.53 mmol) of Fe^{III}(OEP)Cl and 100 mg (5 mmol) of DNOC in dimethylformamide (10 mL) and chloroform (40 mL). The solution was refluxed at 70°C for 3 hours, filtrated, and then divided into five 10-mL vials. The vapor from absolute methanol was allowed to slowly diffuse into the solutions and stand at room temperature. The title compounds were isolated as dark purple block-shaped crystals from a solution of dimethylformamide and chloroform and filtered after 30 days, the product yield was very low.

3.3 Instruments

The stock solution of the sample was prepared and diluted to 4.0 x 10^{-6} M in dimethylsulfoxide before being measured by UV-Vis spectrophotometer and spectrofluorescence. The scanning of UV-Visible spectra was recorded on a Hitachi UH5300 spectrophotometer. The spectrofluorescence spectra scanning was recorded on the JASCO fluorescence spectrometry model FP8000 using excitation wavelength at 538 nm which is corresponded to the major absorption peaks of the porphyrin (Das, 1975). All spectra measuring was carried out at room temperature, and the sample was placed in the 1 cm path length cell quart cuvette. The attenuated Fourier-transform infrared spectroscopy (ATR-FT-IR) was recorded on a Bruker Tensor II spectrometer. The Raman spectra were recorded on Dispersive Raman Microscope, SENTERRA, Bruker by using a 532 nm excitation line. The approximate laser power at the sample was 5 mW with an integration of 3 sec.

3.4 Structure solution and refinement

Crystal data, data collection by using *APEX4*; cell refinement: *SAINT* V8.40B, and data reduction: *SAINT* V8.40B (Bruker, 2021) at room temperature on a Bruker D8 QUEST CMOS PHOTON II diffractometer with graphite monochromatized MoKα (α = 0.71073 Å) X-radiation source. The crystal structure was solved and refined using the *SHELX* program systems (Sheldrick, 2015) through the *ShelXle* (Hübschle et al., 2011) and *Olex2* (Dolomonov et al., 2009) interface tools. The illustrations were produced using *ORTEP-3* (Farrugia, 2012). The final refinement included anisotropic atomic displacement parameters for the non-H atoms. H-atoms were included as geometrically idealized riding model contributors (d[C—$H_{methine}$] = 0.93 Å; (d[C—$H_{methylene}$]) = 0.97 Å; U[H] = with U[H]=1.2U[$C_{attached}$]. Crystal data, data collection, and structure refinement details are summarized in Table 1.

Table 1 Crystal data and experiment details

Crystal data	
Chemical formula	
M_r	785.751
Crystal system, space group	Triclinic, *P*-1
Temperature (K)	296(2)
a, *b*, *c* (Å)	12.522(2) 13.749(2) 14.239(3)
α, β, γ (°)	103.560(5) 114.384(5) 103.173(5)
V (Å^3)	2019.4(6)
Z	2
ρ_{calc}g/cm^{-3}	1.292
Radiation type	Mo *Kα* (α = 0.71073 Å)
μ (mm^{-1})	0.425
Crystal size (mm)	0.34 x 0.20 x 0.10
Data collection	
Diffractometer	Bruker D8 QUEST CMOS PHOTON II, *APEX4* CCD area-detector diffractometer (Bruker, 2021)
Absorption correction	Multi-scan (*SAINT and SADABS*; Bruker, 2016; Bruker, 2021)
T_{min}, T_{max}	
No. of measured, independent and observed [$I > 2\sigma(I)$] reflections	
R_{int}	0.052
Refinement	
$R[F^2 > 2\sigma(F^2)]$, $wR(F^2)$, S	0.042 0.1084 1.036
No. of Reflection	7378
No. of parameters	545
No. of restrains	106
H-atom treatment	Mixed
$\Delta\rho_{max}$, $\Delta\rho_{min}$ (e Å^{-3})	0.49 -0.28

4. Results and discussion

4.1 UV-Visible and fluorescence spectroscopy

The electronic structure of the [Fe^{III}(OEP)(DNOC)] in the solution can be determined by using UV-Vis spectroscopy. The UV-Vis spectrum of [Fe^{III}(OEP)(DNOC)] in DMSO (Figure 2) shows a splitting Soret band at 390 nm and two Q bands at 496 and 604 nm which indicated five-coordinate high-spin, iron(III) porphyrin (Uno, Hatano, Nishimura, & Arata, 1990; Kanamori et al., 2005; Chaudhary, Patra, & Rath, 2010; Bhowmik et al., 2013). The shift of the Soret band in [Fe^{III}(OEP)(DNOC)] was compared with [Fe^{III}(OEP)(2,4,6-trinitrophenol)] (Bhowmik et al., 2013; Puntharod et al., 2017) and [Fe^{III}(OEP)(O-2,6-(i-Pr)$_2$C$_6$H$_3$)](Kanamori et al., 2005). The other phenolate compounds have been seen to exhibit comparable spectroscopic characteristics such as, [Fe^{III}(OEP)Hcat], [Fe^{III}(OEP)OPh], and [Fe^{III}(OEP)OAr] (Chaudhary et al., 2010).

In the present complex, the Soret band and the charge transfer were slightly shifted due to the acidity of the axial ligands. This shift may have been caused by the DNOC's increased aromaticity, which encouraged the creation of intermolecular hydrogen bonds. The shifting of the Soret is dependent on the electron-withdrawing group of the axial ligand, the DNOC compound is substituted by CH_3 on the *para* position causing it less acidity than picrate. The comparison of the acidity of the phenolate ligands found that DNOC (pKa = 4.23) is less acidic than picrate (pKa 0.42) but more acidity than 2,6-diisopropylphenol (pKa 11.1). The highest wavelength of absorption can be proportional to the acidity of the axial phenolate ligand in the region of 380 nm to 650 nm and the creation of hydrogen bonding contacts, according to this result, which was comparable to those of Fe(OEP)phenolate complexes (Uno et al., 1990; Kanamori et al., 2005; Sahoo et al., 2015).

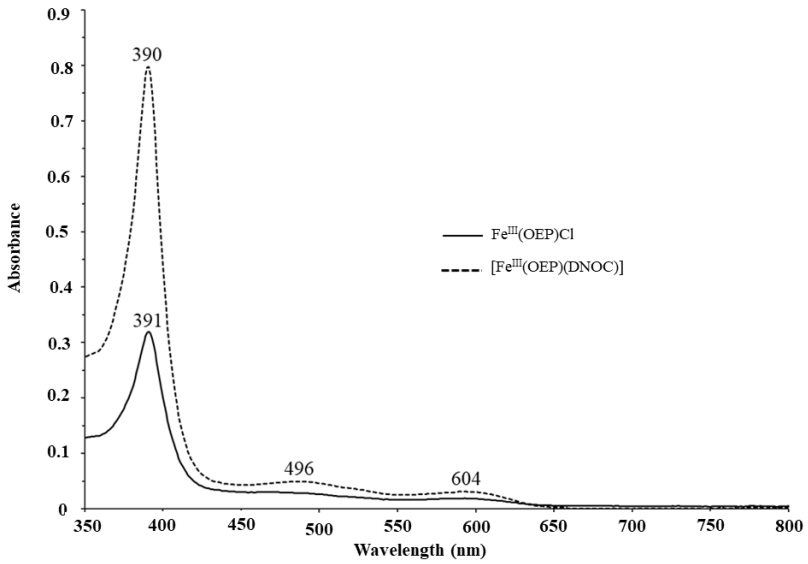

Figure 2 UV-Visible spectra of [Fe^{III}(OEP)(DNOC)] complex in DMSO

Fluorescence emission scanning of the [Fe^{III}(OEP)(DNOC)] complex in DMSO is shown in Figure 3. In this study, the fluorescence emission was shifted from 299 to 326 observed. This result indicated the increase of the emission intensity relative to the ligation of the axial ligand and changes in the charge transfer state. The small λ532 is due to the luminescence of the iron(III) porphyrin (Corwin, 1965). Similar emission spectra of zinc porphyrin complexes have been reported by Das (1975).

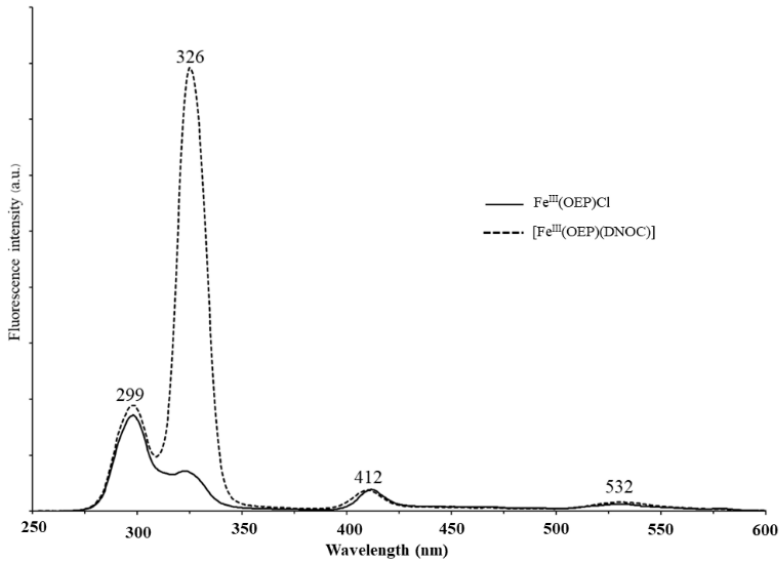

Figure 3 The Fluorescence spectra of [Fe^{III}(OEP)(DNOC)] in DMSO

4.2 FT-IR and Raman spectroscopy

The new complex of [Fe^{III}(OEP)(DNOC)] was initially characterized with ATR-FT-IR spectroscopy. The attenuated total reflection Fourier transform infrared spectra of [Fe^{III}(OEP)(DNOC)] are shown in Figure 4. The [Fe^{III}(OEP)(DNOC)] complex shows new bands near 3419, 1660, 1529, 798, 773, 661, 537, and 401 cm^{-1}, respectively. The formation of the hydrogen bonds in the molecule is observed near 3419 cm^{-1} which is not found in starting material. The explanation seems to be correct, as hydrogen bonding can affect the spectral properties of molecules, leading to changes in the intensity and broadness of certain spectroscopic bands. The strong band near 1660 cm^{-1} indicated the C—O stretching mode and the intermolecular hydrogen bonding in the molecules. The new peak at 1529 cm^{-1} is assigned to the N—O stretching mode of the phenolate plane. The —C—CH$_3$ vibration of the phenolate ring is near 1255 cm^{-1}. The Fe—O mode that appeared at 537 cm^{-1} is like that observed in malaria pigment which showed the Fe—O band near 541 cm^{-1} (Wood et al., 2003) and [Fe^{III}(OEP)(2,4,6-trinitrophenol)] (Puntharod et al., 2017). This result suggested that the increase of the intensities IR spectrum of [Fe^{III}(OEP)(DNOC)] due to the sterically induced rotation of the *para*-CH$_3$ and *ortho*-NO$_2$ functional groups (Puntharod et al., 2017).

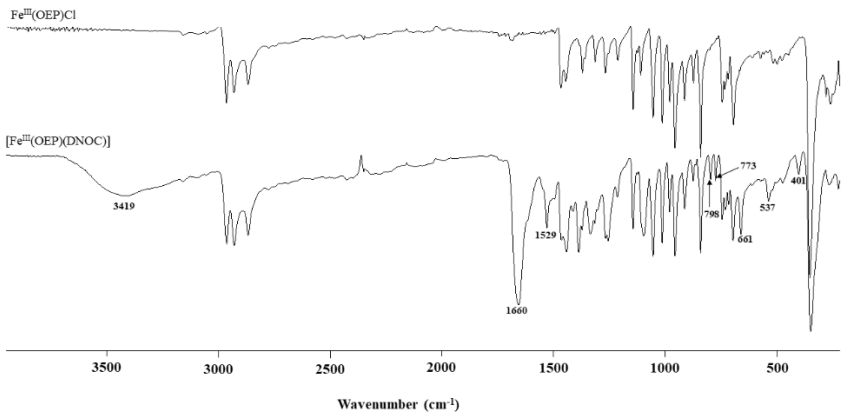

Figure 4 Attenuated total reflection Fourier transform infrared spectra of [Fe^{III}(OEP)(DNOC)]

The Raman spectra of [Fe^{III}(OEP)(DNOC)] were recorded at the excitation wavelength of 532 nm (Figure 5). The Raman spectra of [Fe^{III}(OEP)(DNOC)] exhibit the porphyrin core region 200-2000 cm^{-1} and have been observed by many researchers (Brémard, Kowalewski, Merlin, & Moreau 1992; Hu et al., 1996; Wood et al., 2004). In this present work, the Raman frequencies of [Fe^{III}(OEP)(DNOC)] were compared with [Fe^{III}(OEP)(2,4,6-trinitrophenol)] complex at the excitation wavelength of 514 nm (Puntharod et al., 2017). The result showed that the new ν_4 band near 534 cm^{-1} was assigned as Fe—O bond which this ν_4 band was not found in a starting material, Fe^{III}(OEP)Cl. The ν_4 band has been reported in malaria pigment (hemozoin) by Wood et al. (2003). Furthermore, the ν_4 mode sensitive to the Fe ion oxidative state is observed around 1371 cm^{-1} indicating that the [Fe^{III}(OEP)(DNOC)] complex is a five-coordinate high spin (Brémard et al., 1992). The bands 1625, 1558, 1459, 1308, and 1155 cm^{-1} are mainly associated with the pyrrole ring while the band at 1212 is δ(CmH), these frequencies were found similar with [Fe^{III}(OEP)(2,4,6-trinitrophenol)] (Puntharod et al., 2017).

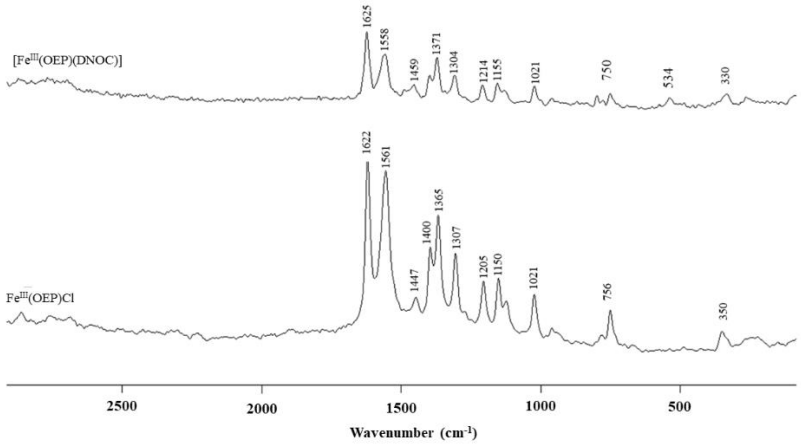

Figure 5 Raman spectra of [Fe^{III}(OEP)(DNOC)]

4.3 Molecular structure

The structure is shown with the atoms labeling (Figure 6) listings of the individual bond distances and bond angles are given in supporting information (S1). Average values for the unique chemical classes of the formal diagram of the porphyrinato core are given in figure 7 which is showed the perpendicular displacements of each atom, in units of 0.01 Å from the mean plane of the 24-atom core. The Fe displacement from the 24-atom plane of 0.41(6) Å is relatively flat which is similar to [Fe^{III}(OEP)(2,4,6-trinitrophenol)] (Bhowmik et al., 2013) and the porphinato core is slightly saddle which the pyrrole nitrogen atoms displacement are out of the mean plane (Mchiri et al., 2019).

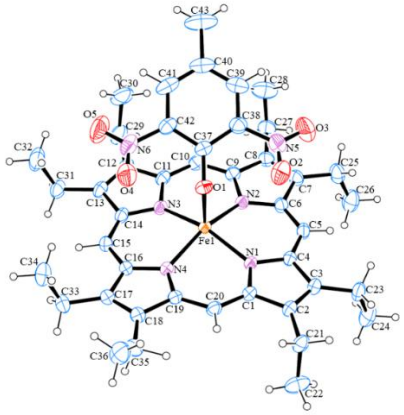

Figure 6 *ORTEP-3* drawing of the [Fe^{III}(OEP)(DNOC)] with the 30% ellipsoids, the atom labeling scheme is also shown

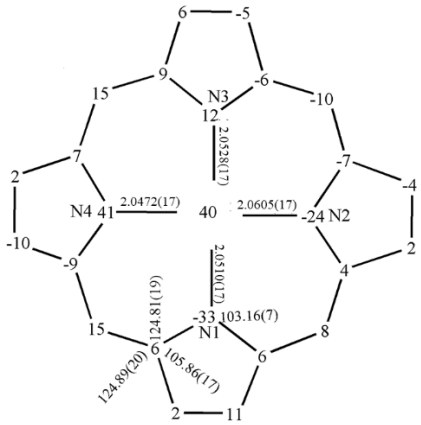

Figure 7 Formal diagram of the porphyrin core displaying perpendicular displacement (in units of 0.01Å) of the core atoms from 24-atoms mean porphyrin plane

The orientation of the DNOC axial ligand covers more than half of the porphyrin core over the N3—Fe1—N2 leading to the dihedral angle (N2—Fe1—C1—O1) and (N3—Fe1—C1—O1) between the DNOC plane and the porphyrin core is 39.99(20)° and -49.3(20), respectively (Figure 8). The orientation of the hydrogen atoms in the methyl group of DNOC at C43 were identified. All three hydrogen atoms were synthesized in various ways and all subtended angles are within 109.47 of their tetrahedral ideal values. A related complexes, [Fe^{III}(OEP)(O-2,6-(i-Pr)$_2$$C_6H_3$)] (Kanamori et al., 2005) and [Fe^{III}(OEP)(2-MeHIm)$_2$]ClO_4 (Scheidt, Geiger, Lee, Reed, & Lang, 1985), with a dihedral angle of 4.32(1) and 3.9° respectively. One hydrogen atom, H43c, is directed away from the porphyrin core. This orientation of the 4-methyl group to minimize the interaction between the bulky CH_3 group of the axial ligand and the porphyrin core (Hu et al., 2018; Scheidt et al., 1985), these steric repulsions induced the changing of the porphyrin core conformation by unequal of Fe—Np bond distance (Norvaiša et al., 2022; Scheidt et al., 1985).

The bonding parameters of axial ligand for the current complex, the Fe—Oax distance of 1.881(15) Å, C1—Oax 1.302(25) Å, and Fe—Oax—C1 of 131.61(14)°, and these parameters were compared to 1.930(13), 1.293(2) and 123.87(2) in [Fe^{III}(OEP)(2,4,6-trinitrophenol)] (Bhowmik et al., 2013) while 1.812(4) Å, 1.332(6) Å and 170.6(4) for [Fe^{III}(OEP)(O-2,6-(i-Pr)$_2$$C_6H_3$)] (Kanamori et al., 2005). The elongation of the present complex was weaker than 2,4,6-tri-tert-butylphenoxyl coordinated with Fe—phthalocyanine (PcFe) complex (Wang, Johnson, Wu, & Ménard, 2021).

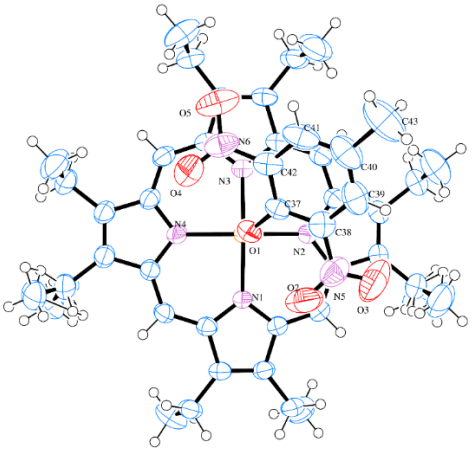

Figure 8 Projection diagram of the orientation of the axial ligand

The Fe—Oax bond distance of the [Fe^{III}(OEP)(DNOC)] is shorter than [Fe^{III}(OEP)(2,4,6-trinitrophenol)] of 0.049 Å but longer than [Fe^{III}(OEP)(O-2,6-(i-Pr)$_2$C$_6$H$_3$)] of 0.065 Å. The comparison of the axial ligand acidity for the three phenolate complexes was found that 2,4,6-trinitrophenol>DNOC>O-2,6-(i-Pr)$_2$C$_6$H$_3$.
The axial ligand parameters for the current molecule is falling in between [Fe^{III}(OEP)(2,4,6-trinitrophenol)] and [Fe^{III}(OEP)(O-2,6-(i-Pr)$_2$C$_6$H$_3$)]. The selected geometric parameters of [Fe^{III}(OEP)(DNOC)] for the phenoxido complexes was shown in Table 2. The Fe—Np bond distances were 2.051(17), 2.060(18), 2.053(18), and 2.047(18) Å, respectively. In the present work, the average Fe—Np bond distance of 2.053(18) Å is in between [Fe^{III}(OEP)(2,4,6-trinitrophenol)] (Bhowmik et al., 2013) and [Fe^{III}(OEP)(O-2,6-(i-Pr)$_2$C$_6$H$_3$)] (Kanamori et al., 2005) complexes. Furthermore, the average Fe—Np bond in [Fe^{III}(OEP)(DNOC)] is slightly longer than the picrate of 0.003 Å but shorter than [Fe^{III}(OEP)(O-2,6-(i-Pr)$_2$C$_6$H$_3$)] of 0.018 Å. It can be seen that these values are found in those related phenolate complexes which this characteristic is commonly found in the five-coordinate high spin iron(III) porphyrin complex (Scheidt, & Lee, 1987)

Table 2 Structural parameters for the iron and axial ligand coordination.

Fe(OEP)Complex	Fe—N_p avg	Fe—24$_{atom}$	Fe—O_{ax}	O_{ax}—C	Fe—O_{ax}—C	references
[Fe^{III}(OEP)(DNOC)]	2.053(18)	0.41(6)	1.881(15)	1.302(25)	131.61(14)	this study
[Fe^{III}(OEP)(O-2,6-(i-Pr)$_2$C$_6$H$_3$)]	2.071(5)	0.54	1.816(4)	1.332(6)	170.60(4)	Kanamori et al., (2005)
[Fe^{III}(OEP)(2,4,6-trinitrophenol)]	2.050(16)	0.40	1.930(13)	1.293(2)	123.87(12)	Bhowmik et al., (2013)

The position of the axial ligand with the interplanar angles from the 24-atom heme plane to the axial ligand C41 plane, the C38—N5—O2, and the C42—N6—O2 plane of 23.8(4), 78.5(3), and -41.0(3)°, respectively. The minimum perpendicular interplanar contacts are 3.368(4) Å at O2, 3.399(5), 3.373(5), and 3.489(5) for O3, O4, and O5 for both nitro groups. The ethyl groups around the porphyrin core point up the axial ligand, and the orientations of the ethyl groups around the porphyrin core are comparable. Due to the disorder at C25 and C35 on the porphyrin plane, six ethyl groups are up and four are down in the current structure. The ethyl groups in Fe^{III}(OEP)Cl (Kohnhorst, & Haller, 2014) and [Fe^{III}(OEP)(O-2,6-(i-Pr)$_2$C$_6$H$_3$)] (Kanamori et al., 2005) were four up, while [Fe^{III}(OEP)(2,4,6-trinitrophenol)] (Bhowmik et al., 2013) were five up. The orientation of ethyl groups is similar in that they are oriented to the side of the axial ligand in both situations, reducing steric hindrance between the porphinato core and the methyl groups (Hu et al., 2018; Scheidt et al., 1985).

The supramolecular dimeric motif in the [Fe^{III}(OEP)(DNOC)] complex was analyzed by

Hirshfeld surface analysis for the study of intermolecular interactions through *CrystalExplorer* systems (Spackman et al., 2021). The plane-plane interactions and the packing molecules were created by the *Mercury* suite (Macrae et. al., 2020) and are reported. Summaries the distribution of individual intermolecular interactions based on fingerprint maps. The red and blue spots on the Hirshfeld surface analysis represent shorter and longer contacts. The white spots suggest contacts with lengths that are equal to the total of the Van der Waals radii (Bondi, 1966). The weak C—H···O hydrogen bonds were detected for intramolecular and intermolecular interactions (Figure 9a-9b).

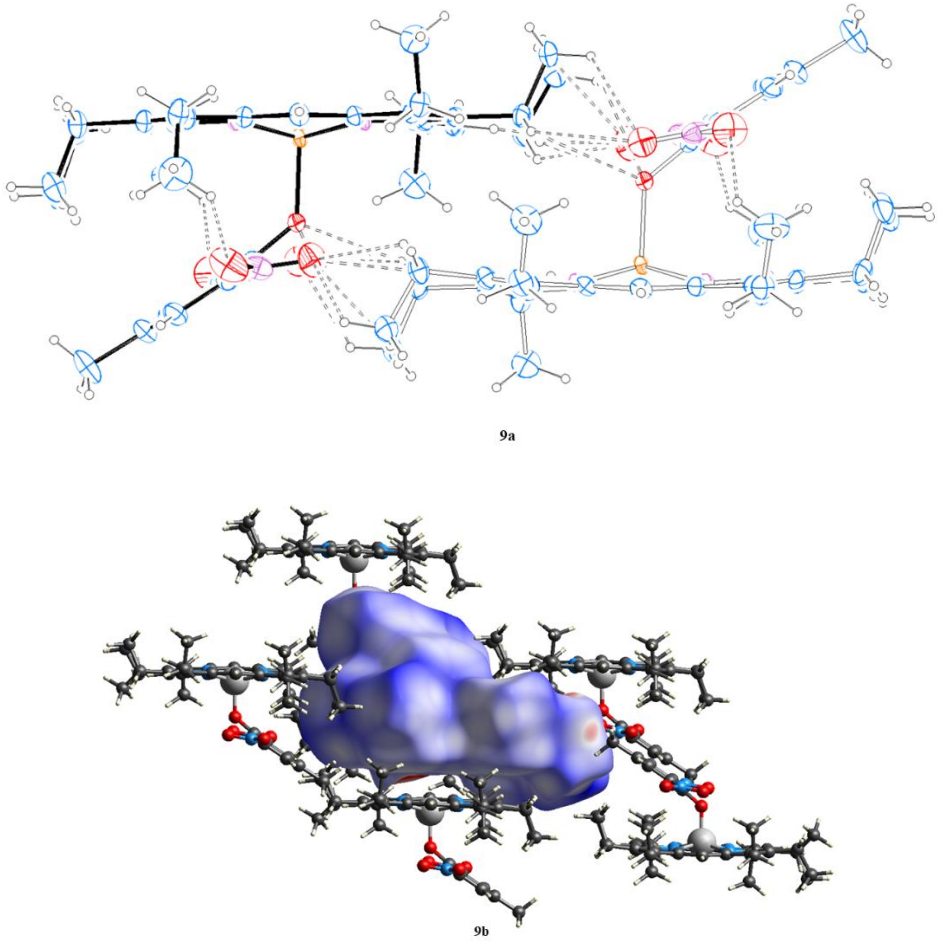

Figure 9 *ORTEP-3* drawing of intermolecular interaction of [Fe^{III}(OEP)(DNOC)] (a) illustrated the C—H···O (b) The closed contacts were in the red spot

The C—H···O hydrogen bonding in crystals has been described by many research groups (Steiner, 2003; Bernstein, Davis, Shimoni, & Chang 1995; Etter, MacDonald, & Bernstein, 1990). In analyzing the [Fe^{III}(OEP)(DNOC)] structure was discovered a new highly concerted group of C—H···O intermolecular interactions (Table 3 and Figure 10), and C—H···π interactions forming a supramolecular dimeric motif. The ethylene H-atoms and methylene H-atom of the porphyrin ring with NO_2 groups of the axial ligand create the C—H···O interactions. The shortest contact, C39—H39···O3 intermolecular interaction distance of 2.732(5) Å was found. The ethylene H-atoms form a C21—H21b···O4 distance of 3.462(4) Å, while the methyl H-atoms form C26—H26c···O4 intramolecular bonded distance of 3.398(4) Å. This dimer has a whopping 20 intermolecular C—H···O

interactions and forms the $R(^{5}_{1})(20)$ motifs (Etter et al., 1990). The methyl group substitute is decreasing the number of hydrogen bond acceptors and forms weak hydrogen bonds in the molecule. The comparison of the number of hydrogen-bonded acceptors in the complexes of [Fe^{III}(OEP)(2,4,6-trinitrophenol)]>[Fe^{III}(OEP)(DNOC)]>[Fe^{III}(OEP)(O-2,6-(i-Pr)$_2C_6H_3$)]. The steric hindrance of the methylene group of DNOC leads the tilting of the axial ligand to minimize the distance between the 4-methyl group and the porphyrin core atoms and reduced the number of hydrogen bond acceptors (Hu et al., 2018; Scheidt et al., 1985).

Table 3 Selected hydrogen-bond parameters (Å) for [Fe^{III}(OEP)(DNOC] complex

D—H···A	D—H	H···A	D···A	D—H···A
C21—H21a···O1	0.97	2.501	3.135(3)	122.84
C21—H21b···O4	0.97	2.770	3.462(4)	128.50
C22—H22b···O4	0.93	2.952	3.498(5)	118.93
C26—H26c···O3	0.97	2.697	3.398(4)	130.30
C32—H32b···O5	0.96	2.588	3.238(4)	125.15
C35—H35···O2	0.96	2.704	3.409(5)	129.93
C39—H39···O3	0.93	2.450	2.732(5)	97.70

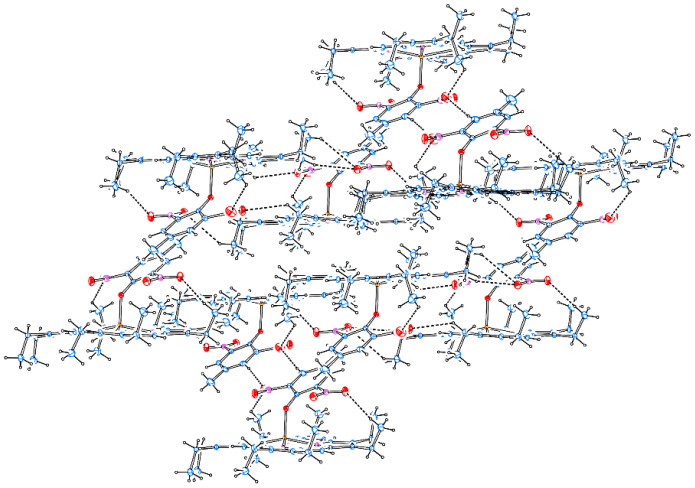

Figure 10 Concerted of C—H···O intermolecular interactions in packing diagram of [Fe^{III}(OEP)(DNOC)] complex

Furthermore, the concerted C—H···π interaction contacts, and π–π stacking has been intensively studied in previous work (Kohnhorst, & Haller, 2014). In this present work, the axial ligand was changed from chloride to DNOC which is rich in oxygen atoms to observe the new supramolecular interaction synthon. A striking supramolecular motif utilizing the OEP face is formed across an inversion center between the bottom of the adjacent OEP-heme. The relative orientation/interaction can be seen in Figures 11 and 12. There are six C—H···π concerted interactions in each of the two dimer structures (the limit of the ring limits such interactions to no more than eight possible). The shortest methyl, C—H···π interactions found from the axial ligand in contact with the inversion-related planes are in the range of 2.61(4)-2.84(5) Å (Figure 13) and the shortest plane-plane contact distance of 3.689(3) Å, these contact interactions are shorter than the [Fe^{III}(OEP)Cl] plane-plane distance (Kohnhorst, & Haller, 2014). The fingerprint shows the dominant contacts in the crystal packing as shown in Figure 14 indicating that the dominant contacts occurred by H···O/O···H contacts (14.3%) and H···H contacts (66.9%). These results suggested that a new high-spin [Fe^{III}(OEP)(DNOC)] complex was packed into a three-dimension supramolecular network by C—H···O, C—H···π, and π–π stacking.

The similarities were found in the low-spin iron(III) bis(4-ethylanilline) complex and high-spin iron(III) bis(aqua) tetra(para-chlorophenyl)porphyrinato and phenazine complex (Dhifaoui et al., 2018a; 2018b) and the six-coordinated Sn(IV)-tetrapyridyl porphyrins (Rani et al., 2018). Another experiment to support the idea that [Fe^{III}(OEP)(DNOC)] was stabilized by the weak hydrogen bonds is the fluorinated porphyrinic crystalline solids which are stabilized by C—F···π, F···F, and C—F···π interactions (Sujatha, & Arunkumar, 2016).

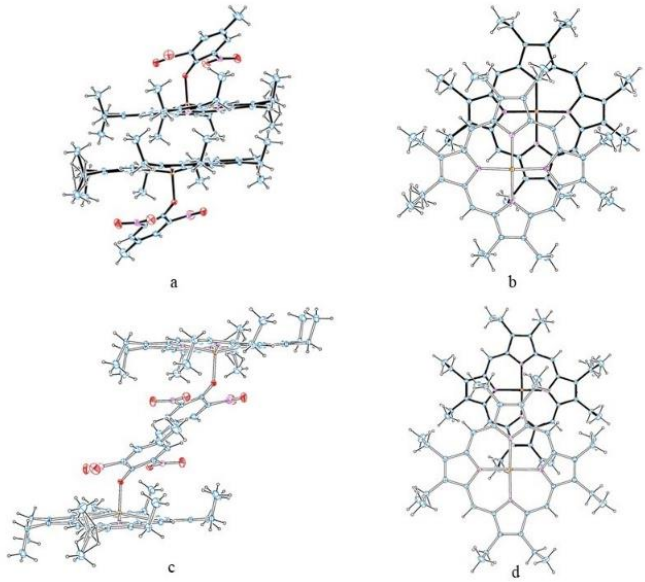

Figure 11 *ORTEP-3* drawing porphyrin face-to-face contact interaction on the opposite side in the molecules. (a) the parallel to the porphyrin plane showing the π–π stackings in the molecule (b) π–π stackings on the axial ligand side (c) the parallel of the porphyrin plane with the axial ligands are encapsulated (d) π–π stackings of the porphyrin plane on the core side

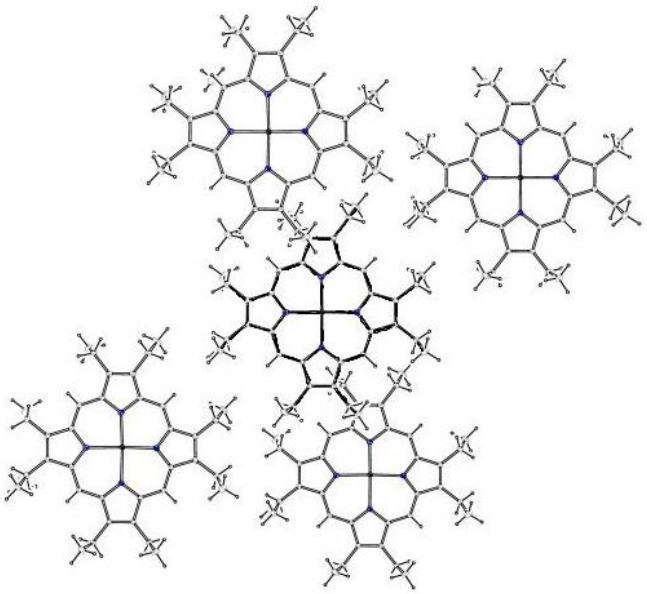

Figure 12 π–π stacking in the five molecules

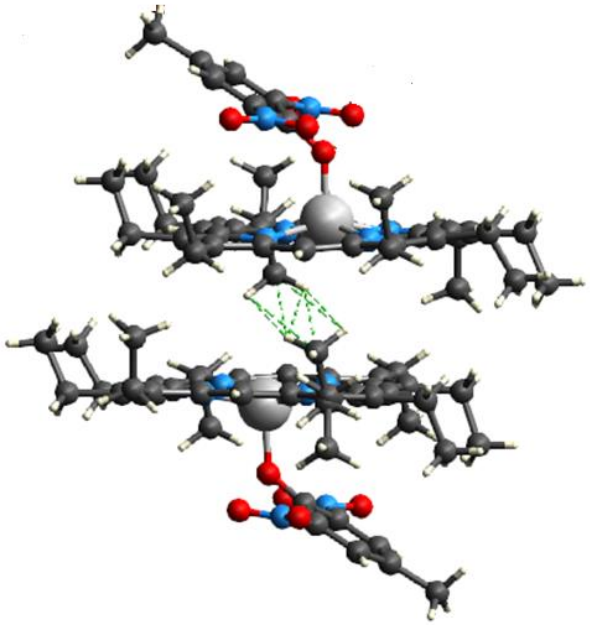

Figure 13 Methyl-methyl short contacts region

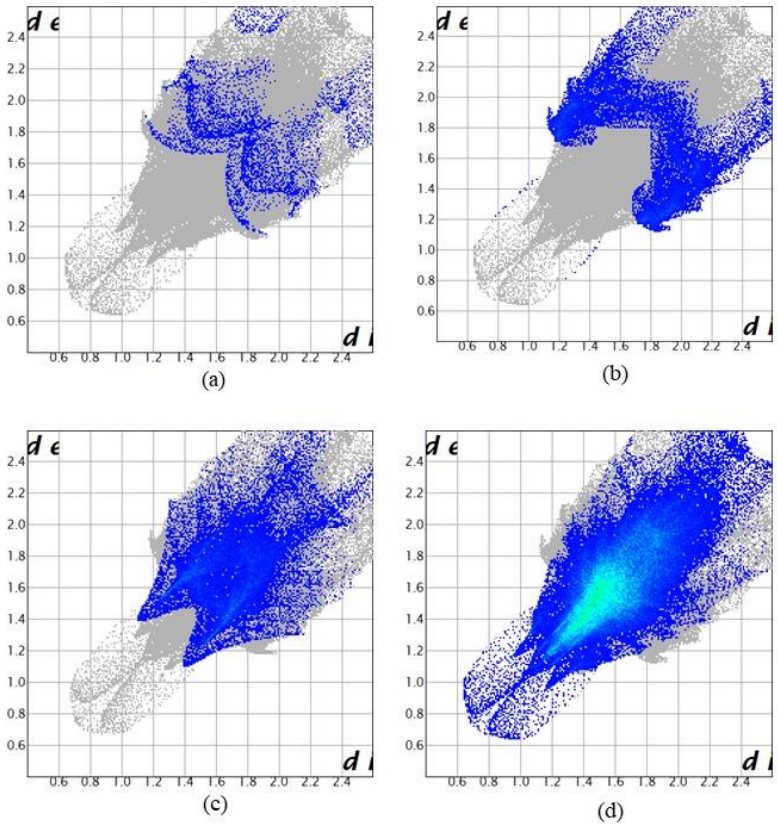

Figure 14 Fingerprint shows the dominant contacts in the molecules (a) N···H/H···N contacts 2.6% (b) C···H/H···C contacts 11.0% (c) H···O/O···H contacts 14.3% (d) H···H contacts 66.9%.

5. Conclusion

In conclusion, the [Fe^{III}(OEP)(DNOC)] complex has six intermolecular C─H···π interactions. This dimer has a whopping 20 intermolecular C─H···O interactions making a total of 26 concerted interactions and firmly establishing this intriguing motif as another supramolecular synthon. This synthon, together with the 3D packing/stacking dominated by porphyrin-porphyrin C─H···π interactions supplemented by axial ligand-porphyrin hydrogen bonding interactions may help explain the similarity of the resonant Raman excitonic enhancement of heme systems.

6. Supplementary Information

Crystallographic data for the structural analysis has been deposited with the Cambridge Crystallographic Data Centre via www.ccdc.cam.ac.uk/structures, CSD 2181506 for the [Fe^{III}(OEP)(DNOC)] complex, the data can be obtained free of charge.

7. Acknowledgements

This study is supported by the Research and Development Institute (RDI) Nakhon Ratchasima Rajabhat University. The authors gratefully acknowledge Associate Professor Dr. Kittipong Chainok at the Thammasat University Research Unit in Multifunctional Crystalline Materials and Applications for collecting crystal structure data.

8. References

Bernstein, J., Davis, R. E., Shimoni, L., & Chang, N.-L. (1995). Patterns in hydrogen bonding: Functionality and graph set analysis in Crystals. *Angewandte Chemie International Edition in English*, *34*(15), 1555–1573. https://doi.org/10.1002/anie.199515551

Bhowmik, S., Dey, S., Sahoo, D., & Rath, S. P. (2013). Unusual stabilization of an intermediate spin state of iron upon the axial phenoxide coordination of a diiron(III)-bisporphyrin: Effect of heme-heme interactions. *Chemistry - A European Journal*, *19*(41), 13732–13744. https://doi.org/10.1002/chem.201301242

Bondi, A. (1966). Van der Waals volumes and radii of metals in covalent compounds. *The Journal of Physical Chemistry*, *70*(9), 3006–3007. https://doi.org/10.1021/j100881a503

Brémard, C., Kowalewski, P., Merlin, J. C., & Moreau, S. (1992). Resonance Raman enhancement of the oxo-bridged dinuclear iron center: Vibrational modes in iron(iii) physiological-type porphyrin complexes. *Journal of Raman Spectroscopy*, *23*(6), 325–333. https://doi.org/10.1002/jrs.1250230603

Bruker. (2016). *APEX4*, *SAINT and SADABS*; Bruker AXS Inc.: Madison, WI, USA.

Bruker. (2021). *SAINT* V8.40B. Bruker AXS Inc. Madison, WI, USA.

Chaudhary, A., Patra, R., & Rath, S. P. (2010). Binding of catechols to iron(iii)–octaethylporphyrin: An experimental and DFT investigation. *European Journal of Inorganic Chemistry*, *2010*(33), 5211–5221. https://doi.org/10.1002/ejic.201000707

Corwin, A. H. (1965). Porphyrins and metalloporphyrins; their general, physical and Coordination Chemistry, and laboratory methods. *Journal of the Amarican Society*, *87*(5), 1154–1155. ttps://doi.org/10.1021/ja01083a061

Das, R. R. (1975). Absorption and emission spectral studies on the dimerization of free porphyrin and its zinc(ii), copper(ii) and nickel(ii) derivatives in aqueous solution. *Journal of Inorganic and Nuclear Chemistry*, *37*(1), 153–157. https://doi.org/10.1016/0022-1902(75)80143-6

Dhifaoui, S., Hajji, M., Nasri, S., Guerfel, T., Daran, J. C., & Nasri, H. (2018b). A new high-spin iron(iii) bis(aqua) complex with the Meso-tetra(para-chlorophenyl)porphyrin: X-ray crystallography, Hirshfeld surface analysis, magnetic, EPR and electrochemical properties. *Research on Chemical Intermediates*, *44*(12), 7259–7276. https://doi.org/10.1007/s11164-018-3555-1

Dhifaoui, S., Mchiri, C., Quatremare, P., Marvaud, V., Bujacz, A., & Nasri, H. (2018a). Molecular structure, magnetic properties, cyclic voltammetry of the low-spin iron(iii) bis(4-ethylaniline) complex with the para -chloro substituted Meso -

tetraphenylporphyrin. *Journal of Molecular Structure*, *1153*, 353–359. https://doi.org/10.1016/j.molstruc.2017.10.023

Dolomanov, O. V., Bourhis, L. J., Gildea, R. J., Howard, J. A., & Puschmann, H. (2009). OLEX2: a complete structure solution, refinement and analysis program. *Journal of applied crystallography*, *42*(2), 339-341. https://doi.org/10.1107/s0021889808042726

Edwards, S. L., Xuong, N. H., Hamlin, R. C., & Kraut, J. (1987). Crystal structure of cytochrome c peroxidase compound I. *Biochemistry*, *26*(6), 1503-1511. https://doi.org/10.1021/bi00380a002

Etter, M. C., MacDonald, J. C., & Bernstein, J. (1990). Graph-set analysis of hydrogen-bond patterns in organic crystals. *Acta Crystallographica Section B: Structural Science*, *46*(2), 256-262. https://doi.org/10.1107/s0108768189012929

Facchin, A., Zerbetto, M., Gennaro, A., Vittadini, A., Forrer, D., & Durante, C. (2021). Oxygen Reduction Reaction at Single-Site Catalysts: A Combined Electrochemical Scanning Tunnelling Microscopy and DFT Investigation on Iron Octaethylporphyrin Chloride on HOPG. *ChemElectroChem*, *8*(15), 2825-2835. https://doi.org/10.1002/celc.202100543

Farrugia, L. J. (1997). *ORTEP*-3 for windows - a version of *ORTEP*-iii with a graphical user interface (GUI). *Journal of Applied Crystallography*, *30*(5), 565–565. https://doi.org/10.1107/s0021889897003117

Hersleth, H.-P., Ryde, U., Rydberg, P., Görbitz, C. H., & Andersson, K. K. (2006). Structures of the high-valent metal-ion haem–oxygen intermediates in peroxidases, oxygenases and catalases. *Journal of Inorganic Biochemistry*, *100*(4), 460–476. https://doi.org/10.1016/j.jinorgbio.2006.01.018

Hu, C., Noll, B. C., Schulz, C. E., & Scheidt, W. R. (2018). Hydrogen-bonding effects in five-coordinate high-spin imidazole-ligated iron(ii) porphyrinates. *Inorganic Chemistry*, *57*(2), 793–803. https://doi.org/10.1021/acs.inorgchem.7b02744

Hu, S., Smith, K. M., & Spiro, T. G. (1996). Assignment of Protoheme Resonance Raman Spectrum by heme labeling in myoglobin. *Journal of the American Chemical Society*, *118*(50), 12638–12646. https://doi.org/10.1021/ja962239e

Hübschle, C. B. (2011). *ShelXle*: A Qt graphical user interface for *SHEXL*. *Acta Crystallographica Section A Foundations and Advances*, *44*, 1281-1284. https://doi.org/10.1107/S0021889811043202

Kanamori, D., Yamada, Y., Onoda, A., Okamura, T.-aki, Adachi, S., Yamamoto, H., & Ueyama, N. (2005). Structures and properties of octaethylporphinato(phenolate)iron(iii) complexes with NH···O hydrogen bonds: Modulation of Fe–O bond character by the hydrogen bond. *Inorganica Chimica Acta*, *358*(2), 331–338. https://doi.org/10.1016/j.ica.2004.09.014

Kingsbury, C. J., & Senge, M. O. (2021). The shape of Porphyrins. *Coordination Chemistry Reviews*, *431*, 213760. https://doi.org/10.1016/j.ccr.2020.213760

Kirkman, H. N., & Gaetani, G. F. (2007). Mammalian catalase: A venerable enzyme with New Mysteries. *Trends in Biochemical Sciences*, *32*(1), 44–50. https://doi.org/10.1016/j.tibs.2006.11.003

Kohnhorst, S. A., & Haller, K. J. (2014). Chlorido(2,3,7,8,12,13,17,18-octaethylporphyrinato)iron(iii): A new triclinic polymorph of Fe(OEP)Cl. *Acta Crystallographica Section C Structural Chemistry*, *70*(4), 368–374. https://doi.org/10.1107/s2053229614005002

Lee, H., Lee, D., Kim, I., Lee, E., & Jang, W.-D. (2020). Formation of supramolecular polymers from porphyrin tripods. *Macromolecules*, *53*(18), 8060–8067. https://doi.org/10.1021/acs.macromol.0c01446

Macrae, C. F., Sovago, I., Cottrell, S. J., Galek, P. T., McCabe, P., Pidcock, E., ... & Wood, P. A. (2020). Mercury 4.0: From

visualization to analysis, design and prediction. *Journal of applied crystallography*, *53*(1), 226-235. https://doi.org/10.1107/s1600576719014092

Martin, D. J., Johnson, S. I., Mercado, B. Q., Raugei, S., & Mayer, J. M. (2020). Intramolecular electrostatic effects on O_2, CO_2, and acetate binding to a cationic iron porphyrin. *Inorganic Chemistry*, *59*(23), 17402–17414. https://doi.org/10.1021/acs.inorgchem.0c02703

Mchiri, C., Dhifaoui, S., Ezzayani, K., Guergueb, M., Roisnel, T., Loiseau, F., & Nasri, H. (2019). Insights into the new cadmium(ii) metalloporphyrin: Synthesis, X-ray crystal structure, Hirshfeld surface analysis, photophysical and cyclic voltammetry characterization of the (morpholine){(meso-tetra(para-chloro-phenyl)porphyrinato}cadmium(ii). *Polyhedron*, *171*, 10–19. https://doi.org/10.1016/j.poly.2019.06.055

Norvaiša, K., Flanagan, K. J., Gibbons, D., & Senge, M. O. (2019). Conformational RE-engineering of porphyrins as receptors with switchable N−H···X-type binding modes. *Angewandte Chemie International Edition*, *58*(46), 16553–16557. https://doi.org/10.1002/anie.201907929

Norvaiša, K., Kielmann, M., & Senge, M. O. (2020). Porphyrins as colorimetric and photometric biosensors in modern bioanalytical systems. *ChemBioChem*, *21*(13), 1793–1807. https://doi.org/10.1002/cbic.202000067

Norvaiša, K., Maguire, S., Donohoe, C., O'Brien, J. E., Twamley, B., Gomes-da-Silva, L. C., & Senge, M. O. (2021). Steric repulsion induced conformational switch in supramolecular structures. *Chemistry – A European Journal*, *28*(4), e202103879. https://doi.org/10.1002/chem.202103879

Panyanon, C., Dungkaew, W., & Chainok, K. (2021, January). Synthesis and structural characterization of $(Na_6F(H_2O)_{18}[(VO_4)_2]$ $\bullet 2H_3O \bullet 2HF$. *Journal of Current Science and Technology*, *11*(1), 32-39. https://doi.org/10.14456/jcst.2021.6

Park, J. M., Hong, K.-I., Lee, H., & Jang, W.-D. (2021). Bioinspired applications of porphyrin derivatives. *Accounts of Chemical Research*, *54*(9), 2249–2260. https://doi.org/10.1021/acs.accounts.1c00114

Puntharod, R. (2008). *Synthesis and structural studies of malaria pigment model systems*. [Doctroal dissertation, Suranaree University of Technology]. http://sutir.sut.ac.th:8080/jspui/handle/123456789/3385

Puntharod, R., Haller, K. J., Robertson, E. G., Gwee, E. S., Izgorodina, E. I., & Wood, B. R. (2017). An improved model for malaria pigment and *β*-hematin: Fe(OEP)Picrate. *Journal of Raman Spectroscopy*, *48*(9), 1148–1157. https://doi.org/10.1002/jrs.5176

Puntharod, R., Webster, G. T., Asghari-Khiavi, M., Bambery, K. R., Safinejad, F., Rivadehi, S., ... & Wood, B. R. (2010). Supramolecular interactions playing an integral role in the near-infrared Raman "excitonic" enhancement observed in β-hematin (malaria pigment) and other related heme derivatives. *The Journal of Physical Chemistry B*, *114*(37), 12104-12115. https://doi.org/10.1021/jp102307s

Rani, J., Raveendran, A., Sushila, Chaudhary, A., Panda, M. K., & Patra, R. (2018). Polymorphism in Sn (IV)-tetrapyridyl porphyrins with a halogenated axial ligand: Structural, photophysical, and morphological study. *Crystal Growth & Design*, *18*(3), 1437-1447. https://doi.org/10.1021/acs.cgd.7b01357

Sahoo, D., Quesne, M. G., de Visser, S. P., & Rath, S. P. (2015). Hydrogen-bonding interactions trigger a spin-flip in iron(III) porphyrin complexes. *Angewandte Chemie International Edition*, *54*, 4796–4800. https://onlinelibrary.wiley.com/doi/10.1002/anie.201411399

Scheidt, W. R., & Lee, Y. J. (1987). Recent advances in the stereochemistry of metallotetrapyrroles. *Structure and Bonding*, 1–70. https://doi.org/10.1007/bfb0036789

Scheidt, W. R., Geiger, D. K., Lee, Y. J., Reed, C. A., & Lang, G. (1985). Characterization of five-coordinate mono (imidazole)(porphinato) iron (II)

complexes. *Journal of the American Chemical Society*, *107*(20), 5693-5699. https://doi.org/10.1021/ja00306a015

Sheldrick, G. M. (2015). Crystal structure refinement with *SHELXL*. *Acta Crystallographica Section C Structural Chemistry*, *71*(1), 3–8. https://doi.org/10.1107/s2053229614024218

Spackman, P. R., Turner, M. J., McKinnon, J. J., Wolff, S. K., Grimwood, D. J., Jayatilaka, D., & Spackman, M. A. (2021). *CrystalExplorer*: A program for Hirshfeld Surface Analysis, visualization and quantitative analysis of molecular crystals. *Journal of Applied Crystallography*, *54*(3), 1006–1011. https://doi.org/10.1107/s1600576721002910

Steiner, T. (2003). C–H···O hydrogen bonding in Crystals. *Crystallography Reviews*, *9*(2-3), 177–228. https://doi.org/10.1080/08893110310001621772

Sujatha, S., & Arunkumar, C. (2016). Fluorinated porphyrinic crystalline solids: Structural elucidation and study of intermolecular interactions. *Crystalline and Non-Crystalline Solids*, 57. https://doi.org/10.5772/62946

Sumner, J. B. (1926). The isolation and crystallization of the enzyme urease. *Journal of Biological Chemistry*, *69*(2), 435–441. https://doi.org/10.1016/s0021-9258(18)84560-4

Sumner, J. B., & Dounce, A. L. (1937). Crystalline catalase. *Science*, *85*(2206), 366–367. https://doi.org/10.1126/science.85.2206.366

Uno, T., Hatano, K., Nishimura, Y., & Arata, Y. (1990). Spectrophotometric and resonance Raman studies on the formation of phenolate and thiolate complexes of (octaethylporphinato)iron(iii). *Inorganic Chemistry*, *29*(15), 2803–2807. https://doi.org/10.1021/ic00340a018

Wang, Z., Johnson, S. I., Wu, G., & Ménard, G. (2021). Multiple N–H and C–H Hydrogen Atom Abstractions Through Coordination-Induced Bond Weakening at Fe-Amine Complexes. *Inorganic Chemistry*, *60*(11), 8242-8251. https://doi.org/10.1021/acs.inorgchem.1c00923

Watanabe, Y., Nakajima, H., & Ueno, T. (2007). Reactivities of oxo and peroxo intermediates studied by hemoprotein mutants. *ChemInform*, *38*(41). https://doi.org/10.1002/chin.200741272

Westrip, S. P. (2010). *publcif*: Software for editing, validating and formatting crystallographic information files. *Journal of Applied Crystallography*, *43*(4), 920–925. https://doi.org/10.1107/s0021889810022120

Wood, B. R., Langford, S. J., Cooke, B. M., Glenister, F. K., Lim, J., & McNaughton, D. (2003). Raman imaging of Hemozoin within the food vacuole of *plasmodium falciparum* trophozoites. *FEBS Letters*, *554*(3), 247–252. https://doi.org/10.1016/s0014-5793(03)00975-x

Wood, B. R., Langford, S. J., Cooke, B. M., Lim, J., Glenister, F. K., Duriska, M., Unthank, J. K., & McNaughton, D. (2004). Resonance Raman spectroscopy reveals new insight into the electronic structure of *β*-hematin and malaria pigment. *Journal of the American Chemical Society*, *126*(30), 9233–9239. https://doi.org/10.1021/ja038691x

Supplementary material

Computing details

Data collection: *APEX4* (Bruker, 2021); cell refinement: *SAINT* V8.40B (Bruker, 2021); data reduction: *SAINT* V8.40B (Bruker, 2021); program(s) used to solve structure: SHELXT (Sheldrick, 2018); program(s) used to refine structure: *SHELXL* 2018/3 (Sheldrick, 2018); molecular graphics: Olex2 1.3 (Dolomanov, Bourhis, Gildea, Howard, & Puschmann, 2009); software used to prepare material for publication: Olex2 1.3 (Dolomanov et al., 2009).

Table S1 Complete Crystallographic Details for [Fe^{III}(OEP)(4-methyl-2,6-dinitrophenol)] Crystal data

$C_{43}H_{49}FeN_6O_5$	***Z* = 2**
M_r = 785.73	F(000) = 830
Triclinic, $P\bar{1}$	D_x = 1.292 Mg m^{-3}
a = 12.522 (2) Å	Mo $K\alpha$ radiation, l = 0.71073 Å
b = 13.749 (2) Å	Cell parameters from 9898 reflections
c = 14.239 (3) Å	q = 3.0–25.7°
a = 103.560 (5)°	m = 0.43 mm^{-1}
b = 114.384 (5)°	T = 296 K
g = 103.173 (5)°	Plate, dark red
V = 2019.4 (6) $Å^3$	0.34 × 0.2 × 0.12 mm
Data collection	
BRUKER D8 QUEST CMOS PHOTON II diffractometer	7378 independent reflections
Radiation source: sealed x-ray tube, Mo	5762 reflections with $I > 2s(I)$
Graphite monochromator	R_{int} = 0.052
Detector resolution: 7.39 pixels mm^{-1}	q_{max} = 25.4°, q_{min} = 3.0°
f and w scans	h = -15→15
Absorption correction: multi-scan *SADABS* (Bruker, 2016; Bruker, 2021) was used for absorption correction. wR2(int) was 0.0631 before and 0.0553 after correction. The Ratio of minimum to maximum transmission is 0.9267. The l/2 correction factor is 0.00150.	k = -16→16
T_{min} = 0.691, T_{max} = 0.745	l = -17→17
38070 measured reflections	
Refinement	
Refinement on F^2	99 restraints
Least-squares matrix: full	Hydrogen site location: inferred from neighbouring sites
$R[F^2 > 2s(F^2)]$ = 0.041	H-atom parameters constrained
$wR(F^2)$ = 0.107	$w = 1/[s^2(F_o^2) + (0.0542P)^2 + 0.4893P]$ where $P = (F_o^2 + 2F_c^2)/3$
S = 1.02	$(D/s)_{max}$ = 0.001
7378 reflections	$D\rho_{max}$ = 0.38 e $Å^{-3}$
545 parameters	$D\rho_{min}$ = -0.19 e $Å^{-3}$

Special details

Geometry. All esds (except the esd in the dihedral angle between two l.s. planes) are estimated using the full covariance matrix. The cell esds are taken into account individually in the estimation of esds in distances, angles, and torsion angles; correlations between esds in cell parameters are only used when they are defined by crystal symmetry. An approximate (isotropic) treatment of cell esds is used for estimating esds involving l.s. planes.

Table S2 Fractional atomic coordinates and isotropic or equivalent isotropic displacement parameters (Å^2) for [Fe^{III}(OEP) (4methyl-2,6-dinitrophenol)]

atom	*x*	*y*	*z*	U_{iso}*/U_{eq}
Fe1	0.61239 (3)	0.40999 (2)	0.39471 (2)	0.03676 (11)
O1	0.63052 (13)	0.39812 (12)	0.26815 (12)	0.0469 (4)
O2	0.7204 (3)	0.2424 (2)	0.2385 (2)	0.1087 (8)
O3	0.5729 (3)	0.0892 (2)	0.1395 (2)	0.1323 (11)
O4	0.5984 (3)	0.56451 (18)	0.2071 (2)	0.0910 (7)
O5	0.4088 (3)	0.5283 (2)	0.0875 (2)	0.1223 (9)
N1	0.76387 (16)	0.38137 (13)	0.49722 (14)	0.0386 (4)
N2	0.50347 (16)	0.25285 (13)	0.35136 (14)	0.0413 (4)
N3	0.44972 (16)	0.44222 (14)	0.34390 (14)	0.0418 (4)
N4	0.71057 (16)	0.57020 (13)	0.48996 (14)	0.0413 (4)
N5	0.6136 (3)	0.1859 (2)	0.1657 (2)	0.0777 (7)
N6	0.4956 (3)	0.5007 (2)	0.1332 (2)	0.0702 (6)
C1	0.8848 (2)	0.45480 (17)	0.56465 (17)	0.0406 (5)
C2	0.9697 (2)	0.40187 (18)	0.60974 (18)	0.0424 (5)
C3	0.8983 (2)	0.29583 (17)	0.56912 (18)	0.0443 (5)
C4	0.7708 (2)	0.28325 (16)	0.49838 (17)	0.0413 (5)
C5	0.6688 (2)	0.18651 (17)	0.43839 (19)	0.0478 (5)
H5	0.685383	0.125137	0.444948	0.057*
C6	0.5451 (2)	0.17176 (17)	0.36994 (19)	0.0454 (5)
C7	0.4415 (2)	0.06889 (18)	0.3058 (2)	0.0531 (6)
C8	0.3379 (2)	0.08897 (18)	0.2493 (2)	0.0519 (6)
C9	0.3766 (2)	0.20383 (17)	0.27790 (18)	0.0451 (5)
C10	0.2978 (2)	0.25831 (19)	0.23954 (19)	0.0494 (6)
H10	0.213824	0.216429	0.187893	0.059*
C11	0.3310 (2)	0.36867 (18)	0.27008 (18)	0.0443 (5)
C12	0.2444 (2)	0.4221 (2)	0.23123 (19)	0.0489 (6)
C13	0.3121 (2)	0.5294 (2)	0.28500 (19)	0.0499 (6)
C14	0.4403 (2)	0.54144 (18)	0.35454 (18)	0.0451 (5)
C15	0.5417 (2)	0.63831 (18)	0.41990 (18)	0.0487 (6)
H15	0.523464	0.700527	0.423377	0.058*
C16	0.6666 (2)	0.65206 (17)	0.48021 (17)	0.0448 (5)
C17	0.7707 (2)	0.75442 (18)	0.53972 (19)	0.0508 (6)
C18	0.8777 (2)	0.73380 (18)	0.58366 (19)	0.0517 (6)
C19	0.8391 (2)	0.61856 (16)	0.55373 (17)	0.0435 (5)
C20	0.9199 (2)	0.56427 (17)	0.58757 (18)	0.0447 (5)
H20	1.005692	0.605286	0.629610	0.054*
C21	1.1081 (2)	0.4568 (2)	0.6879 (2)	0.0529 (6)
H21A	1.140473	0.515622	0.668552	0.064*

Table S2 Continued

atom	*x*	*y*	*z*	U_{iso}*/U_{eq}
H21B	1.149096	0.406233	0.678326	0.064*
C22	1.1425 (3)	0.5004 (3)	0.8083 (2)	0.0836 (9)
H22A	1.109821	0.556085	0.820205	0.125*
H22B	1.232544	0.529371	0.854041	0.125*
H22C	1.107012	0.443508	0.827217	0.125*
C23	0.9402 (2)	0.20685 (19)	0.5956 (2)	0.0577 (6)
H23A	1.029408	0.227286	0.619460	0.069*
H23B	0.895378	0.142659	0.528595	0.069*
C24	0.9178 (3)	0.1812 (3)	0.6845 (3)	0.0858 (10)
H24A	0.829569	0.160474	0.661275	0.129*
H24B	0.964663	0.243512	0.751987	0.129*
H24C	0.944806	0.123172	0.696893	0.129*
C25	0.450 (2)	-0.0392 (11)	0.3074 (15)	0.072 (3)
H25A	0.371007	-0.085528	0.296402	0.087*
H25B	0.516467	-0.029149	0.379265	0.087*
C26	0.4759 (7)	-0.0930 (4)	0.2165 (6)	0.110 (2)
H26A	0.404878	-0.111163	0.144997	0.165*
H26B	0.489814	-0.157135	0.224398	0.165*
H26C	0.549422	-0.044392	0.223112	0.165*
C27	0.2064 (2)	0.0097 (2)	0.1689 (2)	0.0693 (8)
H27A	0.147188	0.039224	0.179843	0.083*
H27B	0.196154	-0.055716	0.184593	0.083*
C28	0.1755 (3)	-0.0175 (3)	0.0499 (3)	0.1103 (13)
H28A	0.091803	-0.070459	0.002466	0.165*
H28B	0.234645	-0.045501	0.038822	0.165*
H28C	0.180136	0.046179	0.032491	0.165*
C29	0.1089 (2)	0.3663 (2)	0.1451 (2)	0.0677 (7)
H29A	0.065476	0.415823	0.149707	0.081*
H29B	0.072089	0.306378	0.160855	0.081*
C30	0.0877 (3)	0.3247 (3)	0.0278 (3)	0.0994 (11)
H30A	-0.000959	0.288422	-0.023432	0.149*
H30B	0.130162	0.275417	0.022411	0.149*
H30C	0.120419	0.383938	0.010268	0.149*
C31	0.2656 (3)	0.6197 (2)	0.2742 (2)	0.0630 (7)
H31A	0.323199	0.683454	0.340447	0.076*
H31B	0.184084	0.600929	0.270636	0.076*
C32	0.2528 (4)	0.6462 (3)	0.1744 (3)	0.0973 (11)
H32A	0.192134	0.584945	0.108037	0.146*

Table S2 Continued

atom	*x*	*y*	*z*	U_{iso}*/U_{eq}
H32B	0.332846	0.664729	0.176834	0.146*
H32C	0.225228	0.705909	0.174522	0.146*
C33	0.7588 (3)	0.86087 (19)	0.5432 (2)	0.0662 (7)
H33A	0.829330	0.917062	0.610763	0.079*
H33B	0.681975	0.860900	0.544451	0.079*
C34	0.7563 (4)	0.8844 (2)	0.4445 (3)	0.0921 (10)
H34A	0.693865	0.824324	0.377690	0.138*
H34B	0.837545	0.896324	0.449826	0.138*
H34C	0.735987	0.947404	0.443072	0.138*
C35	1.0131 (3)	0.8132 (2)	0.6482 (3)	0.0646 (9)
H35A	1.065394	0.779841	0.628995	0.077*
H35B	1.017067	0.875410	0.626879	0.077*
C36	1.0639 (3)	0.8492 (3)	0.7709 (3)	0.0833 (11)
H36A	1.009161	0.877870	0.789728	0.125*
H36B	1.146545	0.903775	0.808282	0.125*
H36C	1.068559	0.789094	0.793537	0.125*
C37	0.5513 (2)	0.34400 (18)	0.16303 (18)	0.0442 (5)
C38	0.5308 (2)	0.2365 (2)	0.1087 (2)	0.0576 (6)
C39	0.4362 (3)	0.1751 (3)	0.0007 (2)	0.0772 (9)
H39	0.425346	0.103565	-0.029941	0.093*
C40	0.3587 (3)	0.2173 (3)	-0.0619 (2)	0.0858 (10)
C41	0.3811 (3)	0.3243 (3)	-0.0151 (2)	0.0750 (9)
H41	0.331883	0.355823	-0.057238	0.090*
C42	0.4748 (2)	0.3865 (2)	0.0930 (2)	0.0538 (6)
C43	0.2521 (4)	0.1501 (4)	-0.1800 (3)	0.149 (2)
H43A	0.275988	0.096843	-0.214642	0.223*
H43B	0.235460	0.195875	-0.221527	0.223*
H43C	0.177560	0.115180	-0.178300	0.223*
C35A	1.0069 (16)	0.8053 (12)	0.6540 (18)	0.058 (7)
H35C	1.008371	0.848645	0.719279	0.069*
H35D	1.051498	0.758964	0.677901	0.069*
C36A	1.088 (3)	0.877 (3)	0.637 (4)	0.082 (11)
H36D	1.040641	0.906570	0.586445	0.123*
H36E	1.129578	0.840778	0.606220	0.123*
H36F	1.149604	0.934571	0.706478	0.123*
C25A	0.457 (4)	-0.0378 (17)	0.299 (2)	0.071 (4)
H25C	0.533974	-0.035922	0.297140	0.085*
H25D	0.386564	-0.094826	0.232620	0.085*

Table S2 Continued

atom	*x*	*y*	*z*	U_{iso}*/U_{eq}
C26A	0.4632 (8)	-0.0580 (6)	0.4010 (7)	0.087 (3)
H26D	0.482970	-0.121217	0.403158	0.131*
H26E	0.383166	-0.068360	0.397859	0.131*
H26F	0.527257	0.002650	0.466486	0.131*

Table S3 Atomic displacement parameters (Å^2) for [Fe^{III}(OEP)(4-methyl-2,6-dinitrophenol)]

atom	U^{11}	U^{22}	U^{33}	U^{12}	U^{13}	U^{23}
Fe1	0.03379 (17)	0.03655 (17)	0.03591 (17)	0.01458 (13)	0.01239 (13)	0.01422 (13)
O1	0.0384 (8)	0.0563 (9)	0.0399 (8)	0.0128 (7)	0.0163 (7)	0.0182 (7)
O2	0.0945 (18)	0.119 (2)	0.114 (2)	0.0699 (17)	0.0345 (16)	0.0462 (17)
O3	0.204 (3)	0.0712 (17)	0.119 (2)	0.0678 (19)	0.069 (2)	0.0333 (15)
O4	0.1013 (18)	0.0708 (14)	0.1019 (17)	0.0358 (13)	0.0457 (15)	0.0373 (13)
O5	0.126 (2)	0.147 (2)	0.139 (2)	0.101 (2)	0.0617 (19)	0.083 (2)
N1	0.0356 (9)	0.0361 (9)	0.0378 (9)	0.0142 (8)	0.0118 (8)	0.0142 (8)
N2	0.0367 (10)	0.0402 (10)	0.0433 (10)	0.0144 (8)	0.0155 (8)	0.0166 (8)
N3	0.0378 (10)	0.0463 (10)	0.0426 (10)	0.0191 (8)	0.0181 (8)	0.0183 (8)
N4	0.0424 (10)	0.0389 (10)	0.0374 (9)	0.0179 (8)	0.0135 (8)	0.0144 (8)
N5	0.101 (2)	0.0721 (18)	0.0699 (16)	0.0458 (16)	0.0443 (16)	0.0246 (14)
N6	0.0792 (17)	0.0966 (19)	0.0773 (16)	0.0541 (16)	0.0508 (15)	0.0575 (16)
C1	0.0385 (11)	0.0451 (12)	0.0386 (11)	0.0169 (10)	0.0169 (9)	0.0188 (10)
C2	0.0374 (11)	0.0511 (13)	0.0449 (12)	0.0212 (10)	0.0198 (10)	0.0236 (10)
C3	0.0413 (12)	0.0477 (13)	0.0503 (13)	0.0232 (10)	0.0219 (10)	0.0233 (11)
C4	0.0413 (12)	0.0405 (12)	0.0425 (12)	0.0185 (10)	0.0180 (10)	0.0177 (10)
C5	0.0482 (13)	0.0390 (12)	0.0558 (13)	0.0214 (11)	0.0213 (11)	0.0198 (11)
C6	0.0455 (13)	0.0385 (12)	0.0512 (13)	0.0163 (10)	0.0225 (11)	0.0167 (10)
C7	0.0482 (14)	0.0386 (12)	0.0587 (14)	0.0102 (10)	0.0205 (12)	0.0123 (11)
C8	0.0428 (13)	0.0456 (13)	0.0531 (14)	0.0087 (11)	0.0183 (11)	0.0123 (11)
C9	0.0396 (12)	0.0466 (13)	0.0452 (12)	0.0128 (10)	0.0192 (10)	0.0168 (10)
C10	0.0324 (11)	0.0573 (14)	0.0506 (13)	0.0116 (10)	0.0155 (10)	0.0212 (11)
C11	0.0377 (12)	0.0574 (14)	0.0454 (12)	0.0222 (11)	0.0212 (10)	0.0252 (11)
C12	0.0386 (12)	0.0693 (16)	0.0527 (13)	0.0275 (12)	0.0254 (11)	0.0322 (12)
C13	0.0488 (13)	0.0674 (16)	0.0527 (13)	0.0346 (13)	0.0290 (12)	0.0330 (12)
C14	0.0467 (13)	0.0556 (14)	0.0457 (12)	0.0301 (11)	0.0246 (11)	0.0254 (11)
C15	0.0572 (14)	0.0466 (13)	0.0472 (13)	0.0298 (12)	0.0238 (12)	0.0187 (11)
C16	0.0542 (14)	0.0396 (12)	0.0373 (11)	0.0213 (11)	0.0181 (10)	0.0131 (10)
C17	0.0611 (15)	0.0410 (13)	0.0430 (12)	0.0213 (11)	0.0190 (11)	0.0135 (10)
C18	0.0569 (13)	0.0402 (12)	0.0482 (13)	0.0164 (10)	0.0186 (11)	0.0154 (10)
C19	0.0443 (12)	0.0385 (12)	0.0379 (11)	0.0138 (10)	0.0128 (10)	0.0137 (9)
C20	0.0370 (11)	0.0437 (12)	0.0423 (12)	0.0109 (10)	0.0113 (10)	0.0172 (10)
C21	0.0357 (12)	0.0616 (15)	0.0595 (15)	0.0198 (11)	0.0179 (11)	0.0275 (12)
C22	0.0454 (15)	0.116 (3)	0.0605 (17)	0.0152 (16)	0.0112 (13)	0.0266 (17)

Table S3 Continued

atom	U^{11}	U^{22}	U^{33}	U^{12}	U^{13}	U^{23}
C23	0.0467 (14)	0.0534 (14)	0.0739 (17)	0.0274 (12)	0.0220 (13)	0.0309 (13)
C24	0.098 (2)	0.083 (2)	0.099 (2)	0.0476 (19)	0.045 (2)	0.062 (2)
C25	0.062 (5)	0.044 (3)	0.097 (5)	0.018 (3)	0.030 (4)	0.020 (3)
C26	0.133 (5)	0.069 (3)	0.141 (5)	0.051 (4)	0.079 (4)	0.026 (3)
C27	0.0516 (15)	0.0538 (16)	0.0728 (18)	0.0055 (12)	0.0179 (14)	0.0125 (14)
C28	0.085 (2)	0.110 (3)	0.071 (2)	0.003 (2)	0.0171 (19)	0.000 (2)
C29	0.0381 (13)	0.0854 (19)	0.085 (2)	0.0290 (13)	0.0251 (14)	0.0438 (16)
C30	0.067 (2)	0.117 (3)	0.069 (2)	0.0228 (19)	0.0014 (16)	0.032 (2)
C31	0.0586 (16)	0.0727 (17)	0.0733 (17)	0.0425 (14)	0.0319 (14)	0.0353 (14)
C32	0.144 (3)	0.101 (2)	0.105 (3)	0.084 (3)	0.074 (3)	0.071 (2)
C33	0.0755 (18)	0.0411 (14)	0.0709 (17)	0.0271 (13)	0.0267 (15)	0.0151 (13)
C34	0.121 (3)	0.0670 (19)	0.099 (2)	0.048 (2)	0.046 (2)	0.0492 (18)
C35	0.0621 (16)	0.0450 (17)	0.0641 (15)	0.0140 (13)	0.0178 (14)	0.0138 (14)
C36	0.065 (2)	0.088 (2)	0.0625 (15)	0.0076 (17)	0.0243 (15)	0.0050 (16)
C37	0.0350 (11)	0.0586 (14)	0.0421 (12)	0.0148 (10)	0.0214 (10)	0.0214 (11)
C38	0.0621 (16)	0.0633 (16)	0.0516 (14)	0.0239 (13)	0.0311 (13)	0.0216 (13)
C39	0.081 (2)	0.0746 (19)	0.0522 (16)	0.0120 (16)	0.0305 (16)	0.0058 (14)
C40	0.076 (2)	0.104 (3)	0.0424 (15)	0.0117 (19)	0.0164 (15)	0.0147 (17)
C41	0.0571 (17)	0.126 (3)	0.0503 (16)	0.0361 (18)	0.0244 (14)	0.0473 (18)
C42	0.0496 (14)	0.0770 (17)	0.0509 (14)	0.0295 (13)	0.0301 (12)	0.0341 (13)
C43	0.113 (3)	0.182 (5)	0.052 (2)	0.013 (3)	-0.004 (2)	0.006 (2)
C35A	0.055 (4)	0.040 (10)	0.067 (9)	0.017 (5)	0.014 (4)	0.030 (8)
C36A	0.075 (11)	0.064 (14)	0.096 (18)	0.012 (8)	0.033 (11)	0.043 (13)
C25A	0.067 (9)	0.043 (4)	0.085 (6)	0.017 (5)	0.026 (6)	0.020 (4)
C26A	0.091 (6)	0.068 (5)	0.115 (6)	0.032 (4)	0.050 (5)	0.054 (4)

Table S4 Geometric parameters (Å, º) for [Fe^{III}(OEP)(4-methyl-2,6-dinitrophenol)]

bond	distance	bond	distance
Fe1—O1	1.8822 (15)	C24—H24A	0.9600
Fe1—N1	2.0510 (17)	C24—H24B	0.9600
Fe1—N2	2.0605 (17)	C24—H24C	0.9600
Fe1—N3	2.0528 (17)	C25—H25A	0.9700
Fe1—N4	2.0472 (17)	C25—H25B	0.9700
O1—C37	1.301 (3)	C25—C26	1.531 (14)
O2—N5	1.213 (3)	C26—H26A	0.9600
O3—N5	1.213 (3)	C26—H26B	0.9600
O4—N6	1.211 (3)	C26—H26C	0.9600
O5—N6	1.212 (3)	C27—H27A	0.9700

Table S4 Continued

bond	distance	bond	distance
N1—C1	1.372 (3)	C27—H27B	0.9700
N1—C4	1.375 (3)	C27—C28	1.502 (4)
N2—C6	1.369 (3)	C28—H28A	0.9600
N2—C9	1.371 (3)	C28—H28B	0.9600
N3—C11	1.365 (3)	C28—H28C	0.9600
N3—C14	1.374 (3)	C29—H29A	0.9700
N4—C16	1.372 (3)	C29—H29B	0.9700
N4—C19	1.371 (3)	C29—C30	1.518 (4)
N5—C38	1.455 (4)	C30—H30A	0.9600
N6—C42	1.459 (4)	C30—H30B	0.9600
C1—C2	1.442 (3)	C30—H30C	0.9600
C1—C20	1.384 (3)	C31—H31A	0.9700
C2—C3	1.358 (3)	C31—H31B	0.9700
C2—C21	1.493 (3)	C31—C32	1.504 (4)
C3—C4	1.435 (3)	C32—H32A	0.9600
C3—C23	1.503 (3)	C32—H32B	0.9600
C4—C5	1.386 (3)	C32—H32C	0.9600
C5—H5	0.9300	C33—H33A	0.9700
C5—C6	1.381 (3)	C33—H33B	0.9700
C6—C7	1.448 (3)	C33—C34	1.503 (4)
C7—C8	1.346 (3)	C34—H34A	0.9600
C7—C25	1.517 (8)	C34—H34B	0.9600
C7—C25A	1.510 (12)	C34—H34C	0.9600
C8—C9	1.443 (3)	C35—H35A	0.9700
C8—C27	1.500 (3)	C35—H35B	0.9700
C9—C10	1.385 (3)	C35—C36	1.495 (4)
C10—H10	0.9300	C36—H36A	0.9600
C10—C11	1.385 (3)	C36—H36B	0.9600
C11—C12	1.441 (3)	C36—H36C	0.9600
C12—C13	1.358 (3)	C37—C38	1.406 (3)
C12—C29	1.489 (3)	C37—C42	1.411 (3)
C13—C14	1.441 (3)	C38—C39	1.382 (4)
C13—C31	1.500 (3)	C39—H39	0.9300
C14—C15	1.387 (3)	C39—C40	1.364 (5)
C15—H15	0.9300	C40—C41	1.373 (5)
C15—C16	1.378 (3)	C40—C43	1.523 (4)
C16—C17	1.446 (3)	C41—H41	0.9300
C17—C18	1.353 (3)	C41—C42	1.383 (4)

Table S4 Continued

bond	distance	bond	distance
C17—C33	1.496 (3)	C43—H43A	0.9600
C18—C19	1.446 (3)	C43—H43B	0.9600
C18—C35	1.519 (4)	C43—H43C	0.9600
C18—C35A	1.436 (19)	C35A—H35C	0.9700
C19—C20	1.387 (3)	C35A—H35D	0.9700
C20—H20	0.9300	C35A—C36A	1.388 (19)
C21—H21A	0.9700	C36A—H36D	0.9600
C21—H21B	0.9700	C36A—H36E	0.9600
C21—C22	1.508 (4)	C36A—H36F	0.9600
C22—H22A	0.9600	C25A—H25C	0.9700
C22—H22B	0.9600	C25A—H25D	0.9700
C22—H22C	0.9600	C25A—C26A	1.51 (2)
C23—H23A	0.9700	C26A—H26D	0.9600
C23—H23B	0.9700	C26A—H26E	0.9600
C23—C24	1.505 (4)	C26A—H26F	0.9600

Table S5 Bond angles for [Fe^{III}(OEP)(4-methyl-2,6-dinitrophenol)]

angle	degree	angle	degree
O1—Fe1—N1	103.19 (7)	C7—C25—C26	111.1 (8)
O1—Fe1—N2	100.05 (7)	H25A—C25—H25B	108.0
O1—Fe1—N3	99.20 (7)	C26—C25—H25A	109.4
O1—Fe1—N4	102.33 (7)	C26—C25—H25B	109.4
N1—Fe1—N2	87.81 (7)	C25—C26—H26A	109.5
N1—Fe1—N3	157.60 (7)	C25—C26—H26B	109.5
N3—Fe1—N2	87.65 (7)	C25—C26—H26C	109.5
N4—Fe1—N1	87.66 (7)	H26A—C26—H26B	109.5
N4—Fe1—N2	157.61 (7)	H26A—C26—H26C	109.5
N4—Fe1—N3	88.24 (7)	H26B—C26—H26C	109.5
C37—O1—Fe1	131.59 (14)	C8—C27—H27A	109.0
C1—N1—Fe1	126.03 (13)	C8—C27—H27B	109.0
C1—N1—C4	105.81 (16)	C8—C27—C28	113.0 (3)
C4—N1—Fe1	127.28 (14)	H27A—C27—H27B	107.8
C6—N2—Fe1	127.02 (14)	C28—C27—H27A	109.0
C6—N2—C9	105.77 (17)	C28—C27—H27B	109.0
C9—N2—Fe1	125.87 (14)	C27—C28—H28A	109.5
C11—N3—Fe1	125.60 (14)	C27—C28—H28B	109.5
C11—N3—C14	105.92 (17)	C27—C28—H28C	109.5
C14—N3—Fe1	126.73 (14)	H28A—C28—H28B	109.5
C16—N4—Fe1	126.42 (14)	H28A—C28—H28C	109.5

Table S5 Continued

angle	degree	angle	degree
C19—N4—Fe1	125.71 (14)	H28B—C28—H28C	109.5
C19—N4—C16	105.83 (17)	C12—C29—H29A	108.9
O2—N5—O3	122.5 (3)	C12—C29—H29B	108.9
O2—N5—C38	118.7 (3)	C12—C29—C30	113.5 (2)
O3—N5—C38	118.8 (3)	H29A—C29—H29B	107.7
O4—N6—O5	122.4 (3)	C30—C29—H29A	108.9
O4—N6—C42	119.9 (2)	C30—C29—H29B	108.9
O5—N6—C42	117.7 (3)	C29—C30—H30A	109.5
N1—C1—C2	110.34 (18)	C29—C30—H30B	109.5
N1—C1—C20	124.77 (19)	C29—C30—H30C	109.5
C20—C1—C2	124.9 (2)	H30A—C30—H30B	109.5
C1—C2—C21	125.2 (2)	H30A—C30—H30C	109.5
C3—C2—C1	106.49 (19)	H30B—C30—H30C	109.5
C3—C2—C21	128.3 (2)	C13—C31—H31A	108.7
C2—C3—C4	107.19 (18)	C13—C31—H31B	108.7
C2—C3—C23	127.7 (2)	C13—C31—C32	114.4 (2)
C4—C3—C23	125.0 (2)	H31A—C31—H31B	107.6
N1—C4—C3	110.16 (18)	C32—C31—H31A	108.7
N1—C4—C5	124.43 (19)	C32—C31—H31B	108.7
C5—C4—C3	125.4 (2)	C31—C32—H32A	109.5
C4—C5—H5	116.6	C31—C32—H32B	109.5
C6—C5—C4	126.8 (2)	C31—C32—H32C	109.5
C6—C5—H5	116.6	H32A—C32—H32B	109.5
N2—C6—C5	124.5 (2)	H32A—C32—H32C	109.5
N2—C6—C7	110.2 (2)	H32B—C32—H32C	109.5
C5—C6—C7	125.3 (2)	C17—C33—H33A	109.3
C6—C7—C25	125.7 (10)	C17—C33—H33B	109.3
C6—C7—C25A	123.7 (16)	C17—C33—C34	111.4 (2)
C8—C7—C6	106.8 (2)	H33A—C33—H33B	108.0
C8—C7—C25	127.5 (10)	C34—C33—H33A	109.3
C8—C7—C25A	129.3 (15)	C34—C33—H33B	109.3
C7—C8—C9	107.0 (2)	C33—C34—H34A	109.5
C7—C8—C27	128.1 (2)	C33—C34—H34B	109.5
C9—C8—C27	124.9 (2)	C33—C34—H34C	109.5
N2—C9—C8	110.30 (19)	H34A—C34—H34B	109.5
N2—C9—C10	124.2 (2)	H34A—C34—H34C	109.5
C10—C9—C8	125.5 (2)	H34B—C34—H34C	109.5
C9—C10—H10	116.6	C18—C35—H35A	109.2
C9—C10—C11	126.8 (2)	C18—C35—H35B	109.2
C11—C10—H10	116.6	H35A—C35—H35B	107.9
N3—C11—C10	124.65 (19)	C36—C35—C18	112.2 (3)
N3—C11—C12	110.50 (19)	C36—C35—H35A	109.2
C10—C11—C12	124.8 (2)	C36—C35—H35B	109.2
C11—C12—C29	124.8 (2)	C35—C36—H36A	109.5
C13—C12—C11	106.6 (2)	C35—C36—H36B	109.5
C13—C12—C29	128.6 (2)	C35—C36—H36C	109.5
C12—C13—C14	106.8 (2)	H36A—C36—H36B	109.5
C12—C13—C31	127.7 (2)	H36A—C36—H36C	109.5

Table S5 Continued

angle	degree	angle	degree
C14—C13—C31	125.5 (2)	H36B—C36—H36C	109.5
N3—C14—C13	110.1 (2)	O1—C37—C38	123.3 (2)
N3—C14—C15	124.2 (2)	O1—C37—C42	123.3 (2)
C15—C14—C13	125.6 (2)	C38—C37—C42	113.3 (2)
C14—C15—H15	116.6	C37—C38—N5	119.7 (2)
C16—C15—C14	126.8 (2)	C39—C38—N5	117.0 (3)
C16—C15—H15	116.6	C39—C38—C37	123.2 (3)
N4—C16—C15	124.9 (2)	C38—C39—H39	119.3
N4—C16—C17	110.0 (2)	C40—C39—C38	121.4 (3)
C15—C16—C17	125.1 (2)	C40—C39—H39	119.3
C16—C17—C33	124.9 (2)	C39—C40—C41	117.5 (3)
C18—C17—C16	107.2 (2)	C39—C40—C43	122.0 (4)
C18—C17—C33	127.8 (2)	C41—C40—C43	120.5 (4)
C17—C18—C19	106.4 (2)	C40—C41—H41	119.1
C17—C18—C35	128.0 (2)	C40—C41—C42	121.7 (3)
C17—C18—C35A	130.8 (5)	C42—C41—H41	119.1
C19—C18—C35	125.5 (2)	C37—C42—N6	119.9 (2)
C35A—C18—C19	122.7 (5)	C41—C42—N6	117.6 (2)
N4—C19—C18	110.57 (19)	C41—C42—C37	122.5 (3)
N4—C19—C20	124.42 (19)	C40—C43—H43A	109.5
C20—C19—C18	125.0 (2)	C40—C43—H43B	109.5
C1—C20—C19	126.1 (2)	C40—C43—H43C	109.5
C1—C20—H20	116.9	H43A—C43—H43B	109.5
C19—C20—H20	116.9	H43A—C43—H43C	109.5
C2—C21—H21A	108.8	H43B—C43—H43C	109.5
C2—C21—H21B	108.8	C18—C35A—H35C	104.1
C2—C21—C22	113.9 (2)	C18—C35A—H35D	104.1
H21A—C21—H21B	107.7	H35C—C35A—H35D	105.5
C22—C21—H21A	108.8	C36A—C35A—C18	132 (2)
C22—C21—H21B	108.8	C36A—C35A—H35C	104.1
C21—C22—H22A	109.5	C36A—C35A—H35D	104.1
C21—C22—H22B	109.5	C35A—C36A—H36D	109.5
C21—C22—H22C	109.5	C35A—C36A—H36E	109.5
H22A—C22—H22B	109.5	C35A—C36A—H36F	109.5
H22A—C22—H22C	109.5	H36D—C36A—H36E	109.5
H22B—C22—H22C	109.5	H36D—C36A—H36F	109.5
C3—C23—H23A	108.9	H36E—C36A—H36F	109.5
C3—C23—H23B	108.9	C7—C25A—H25C	110.1
C3—C23—C24	113.2 (2)	C7—C25A—H25D	110.1
H23A—C23—H23B	107.8	C7—C25A—C26A	108.0 (12)
C24—C23—H23A	108.9	H25C—C25A—H25D	108.4
C24—C23—H23B	108.9	C26A—C25A—H25C	110.1
C23—C24—H24A	109.5	C26A—C25A—H25D	110.1
C23—C24—H24B	109.5	C25A—C26A—H26D	109.5
C23—C24—H24C	109.5	C25A—C26A—H26E	109.5
H24A—C24—H24B	109.5	C25A—C26A—H26F	109.5
H24A—C24—H24C	109.5	H26D—C26A—H26E	109.5

Table S5 Continued

angle	degree	angle	degree
H24B—C24—H24C	109.5	H26D—C26A—H26F	109.5
C7—C25—H25A	109.4	H26E—C26A—H26F	109.5
C7—C25—H25B	109.4		
Fe1—O1—C37—C38	-86.8 (3)	C8—C7—C25—C26	90.6 (15)
Fe1—O1—C37—C42	91.4 (3)	C8—C7—C25A—C26A	-105 (2)
Fe1—N1—C1—C2	-170.15 (14)	C8—C9—C10—C11	176.3 (2)
Fe1—N1—C1—C20	10.9 (3)	C9—N2—C6—C5	179.1 (2)
Fe1—N1—C4—C3	170.46 (14)	C9—N2—C6—C7	0.3 (2)
Fe1—N1—C4—C5	-8.8 (3)	C9—C8—C27—C28	80.8 (4)
Fe1—N2—C6—C5	11.8 (3)	C9—C10—C11—N3	0.5 (4)
Fe1—N2—C6—C7	-166.98 (15)	C9—C10—C11—C12	-177.4 (2)
Fe1—N2—C9—C8	167.18 (15)	C10—C11—C12—C13	176.6 (2)
Fe1—N2—C9—C10	-14.2 (3)	C10—C11—C12—C29	-5.6 (4)
Fe1—N3—C11—C10	17.2 (3)	C11—N3—C14—C13	-0.2 (2)
Fe1—N3—C11—C12	-164.65 (14)	C11—N3—C14—C15	-177.9 (2)
Fe1—N3—C14—C13	165.31 (14)	C11—C12—C13—C14	1.4 (2)
Fe1—N3—C14—C15	-12.4 (3)	C11—C12—C13—C31	-179.7 (2)
Fe1—N4—C16—C15	13.9 (3)	C11—C12—C29—C30	-76.1 (3)
Fe1—N4—C16—C17	-164.43 (15)	C12—C13—C14—N3	-0.8 (3)
Fe1—N4—C19—C18	163.58 (15)	C12—C13—C14—C15	176.9 (2)
Fe1—N4—C19—C20	-18.4 (3)	C12—C13—C31—C32	-80.4 (4)
O1—C37—C38—N5	-9.7 (4)	C13—C12—C29—C30	101.2 (3)
O1—C37—C38—C39	172.0 (2)	C13—C14—C15—C16	-174.5 (2)
O1—C37—C42—N6	9.2 (3)	C14—N3—C11—C10	-177.1 (2)
O1—C37—C42—C41	-172.4 (2)	C14—N3—C11—C12	1.1 (2)
O2—N5—C38—C37	-26.2 (4)	C14—C13—C31—C32	98.3 (3)
O2—N5—C38—C39	152.2 (3)	C14—C15—C16—N4	-3.7 (4)
O3—N5—C38—C37	153.0 (3)	C14—C15—C16—C17	174.4 (2)
O3—N5—C38—C39	-28.6 (4)	C15—C16—C17—C18	-177.2 (2)
O4—N6—C42—C37	24.9 (4)	C15—C16—C17—C33	-1.1 (4)
O4—N6—C42—C41	-153.6 (3)	C16—N4—C19—C18	-1.0 (2)
O5—N6—C42—C37	-157.7 (3)	C16—N4—C19—C20	177.1 (2)
O5—N6—C42—C41	23.8 (4)	C16—C17—C18—C19	-1.6 (3)
N1—Fe1—O1—C37	130.05 (19)	C16—C17—C18—C35	176.3 (3)
N1—C1—C2—C3	-0.3 (2)	C16—C17—C18—C35A	-176.9 (11)
N1—C1—C2—C21	-179.0 (2)	C16—C17—C33—C34	-84.8 (3)
N1—C1—C20—C19	5.1 (4)	C17—C18—C19—N4	1.6 (3)
N1—C4—C5—C6	-1.0 (4)	C17—C18—C19—C20	-176.4 (2)
N2—Fe1—O1—C37	39.9 (2)	C17—C18—C35—C36	95.4 (4)
N2—C6—C7—C8	-0.2 (3)	C17—C18—C35A—C36A	-66 (3)
N2—C6—C7—C25	-177.9 (6)	C18—C17—C33—C34	90.5 (3)
N2—C6—C7—C25A	174.4 (10)	C18—C19—C20—C1	176.6 (2)
N2—C9—C10—C11	-2.1 (4)	C19—N4—C16—C15	178.2 (2)
N3—Fe1—O1—C37	-49.3 (2)	C19—N4—C16—C17	0.0 (2)
N3—C11—C12—C13	-1.6 (3)	C19—C18—C35—C36	-87.1 (3)
N3—C11—C12—C29	176.2 (2)	C19—C18—C35A—C36A	119 (3)
N3—C14—C15—C16	2.9 (4)	C20—C1—C2—C3	178.6 (2)
N4—Fe1—O1—C37	-139.48 (19)	C20—C1—C2—C21	0.0 (4)

Table S5 Continued

angle	degree	angle	degree
N4—C16—C17—C18	1.1 (3)	C21—C2—C3—C4	179.4 (2)
N4—C16—C17—C33	177.2 (2)	C21—C2—C3—C23	2.1 (4)
N4—C19—C20—C1	-1.1 (4)	C23—C3—C4—N1	176.3 (2)
N5—C38—C39—C40	-176.0 (3)	C23—C3—C4—C5	-4.4 (4)
C1—N1—C4—C3	0.8 (2)	C25—C7—C8—C9	177.6 (7)
C1—N1—C4—C5	-178.5 (2)	C25—C7—C8—C27	-3.8 (8)
C1—C2—C3—C4	0.8 (2)	C27—C8—C9—N2	-178.5 (2)
C1—C2—C3—C23	-176.5 (2)	C27—C8—C9—C10	3.0 (4)
C1—C2—C21—C22	85.7 (3)	C29—C12—C13—C14	-176.3 (2)
C2—C1—C20—C19	-173.7 (2)	C29—C12—C13—C31	2.6 (4)
C2—C3—C4—N1	-1.0 (3)	C31—C13—C14—N3	-179.7 (2)
C2—C3—C4—C5	178.2 (2)	C31—C13—C14—C15	-2.1 (4)
C2—C3—C23—C24	96.3 (3)	C33—C17—C18—C19	-177.6 (2)
C3—C2—C21—C22	-92.7 (3)	C33—C17—C18—C35	0.3 (5)
C3—C4—C5—C6	179.8 (2)	C33—C17—C18—C35A	7.1 (11)
C4—N1—C1—C2	-0.3 (2)	C35—C18—C19—N4	-176.3 (3)
C4—N1—C1—C20	-179.3 (2)	C35—C18—C19—C20	5.7 (4)
C4—C3—C23—C24	-80.5 (3)	C37—C38—C39—C40	2.4 (5)
C4—C5—C6—N2	-0.6 (4)	C38—C37—C42—N6	-172.5 (2)
C4—C5—C6—C7	178.0 (2)	C38—C37—C42—C41	6.0 (3)
C5—C6—C7—C8	-179.0 (2)	C38—C39—C40—C41	2.5 (5)
C5—C6—C7—C25	3.3 (7)	C38—C39—C40—C43	-178.5 (3)
C5—C6—C7—C25A	-4.5 (10)	C39—C40—C41—C42	-2.8 (5)
C6—N2—C9—C8	-0.3 (2)	C40—C41—C42—N6	176.8 (3)
C6—N2—C9—C10	178.3 (2)	C40—C41—C42—C37	-1.6 (4)
C6—C7—C8—C9	0.0 (3)	C42—C37—C38—N5	172.0 (2)
C6—C7—C8—C27	178.6 (3)	C42—C37—C38—C39	-6.3 (4)
C6—C7—C25—C26	-92.2 (14)	C43—C40—C41—C42	178.1 (3)
C6—C7—C25A—C26A	82 (2)	C35A—C18—C19—N4	177.5 (10)
C7—C8—C9—N2	0.2 (3)	C35A—C18—C19—C20	-0.5 (10)
C7—C8—C9—C10	-178.4 (2)	C25A—C7—C8—C9	-174.1 (11)
C7—C8—C27—C28	-97.6 (4)	C25A—C7—C8—C27	4.4 (12)

Document origin: *publCIF* (Westrip, 2010)